(36)

A Method to Analyze the Malignant Potential of Colorectal Polyps Using Endoscopic Images

by

Matthew J. Emerson
BS, Electrical Engineering, Northeastern University, 1996
Submitted to the Department of Electrical Engineering and Computer Science
in Partial Fulfillment of the Requirements for the Degree of
Master of Science in Electrical Engineering

at the

Massachusetts Institute of Technology

June 1998

Signature of Author:_____
Department of Electrical Engineering and Computer Science
22 May 1998

Approved by:_____
Homer H. Pien, PhD
Technical Supervisor, Draper Laboratory

Certified by:_____
W. Clement Karl
Assistant Professor, Boston University
Research Associate, Laboratory for Information and Decision Systems
Thesis Supervisor

Accepted by:_____
Professor A. C. Smith
Chair, Committee on Graduate Students

A Method to Analyze the Malignant Potential of Colorectal Polyps Using Endoscopic Images

by

Matthew J. Emerson

Submitted to the Department of Electrical Engineering and Computer Science
on 22 May 1998 in Partial Fulfillment of the
Requirements for the Degree of Master of Science in
Electrical Engineering

Abstract

This thesis describes a method to classify colorectal polyps in vivo. The two types of polyps under consideration are hyperplastic polyps (non-neoplastic) and adenomatous polyps (neoplastic). Neoplastic polyps are potentially malignant. Non-neoplastic polyps are benign. The proposed method described herein is a safer and more cost effective alternative to current histologic techniques, since no excision of the polyp needs to be performed. To obtain the information to classify the polyp, we calculate a set of features describing the polyp. The features considered are the texture and color of the polyp's surface, the polyp's size, the location of the polyp in the colon, and the age of patient. These features are either known a priori or are obtained from a digital image of the polyp acquired during endoscopy. The features acquired from a set of training images were used to calculate the weights for a linear discriminant function. Once the weights of this function were calculated, the function was applied to a set of test images and the performance of the algorithm was evaluated for both the test set and the training set. From this calculation, different sized subsets of the features were considered in order to determine the reduced feature set which provided the optimal discrimination. It was found that texture played the most important role in the discrimination. While the work described herein can benefit from having a larger sample of images, we nonetheless found that we were able to classify correctly 65% to 82.5% of the images viewed in the training set.

Thesis Supervisor: W. Clement Karl
Title: Research Associate, Laboratory for Information and Decision Systems

Acknowledgement

I would like to express my great thanks and appreciation to all those who have helped me through this thesis.

First and foremost, I would like to thank my thesis advisors, Homer Pien of Draper Laboratory and Clem Karl of Boston University. Their support and advice helped me through more than one roadblock in the process of completing this thesis.

This work would not have been possible without the assistance and the encouragement of the people at Massachusetts General Hospital: Norm Nishioka, Mary-Ann Mycek, and Bill Purricelli. Without Norm's advice I may never have considered choosing this thesis topic, without the help of Mary-Ann I may never have understood some of the concepts behind the problem, and without Bill's help I may never have received the data to process.

For all the other people who have helped me through this, you have my thanks. To my friends at Draper Labs, Mukund Desai and Anthony Sacramone, you always made yourselves available when I needed assistance. I truly appreciated the time I spent with both of you. To Dave and Mary-Beth, you always gave me someone I could talk to. To my family, I could not have gone so far if you had not always believed that I could.

Finally, thank you Mary, for putting up with me while I have pursued my dream. Without your support and understanding, none of this would have been possible.

This thesis was prepared with the generous support of the Charles Stark Draper Laboratoy, Inc. through the Internal Research and Development Program.

Contents

List of Tables

List of Figures

Chapter 1

Introduction

1.1 Overview

Excluding nonmelanoma skin cancer, colorectal cancer is the second most common form of cancer in the United States, and, globally, it is the third most common in males and fourth most common in females. It is estimated that 6% of the American population will eventually develop colorectal cancer, and 6 million Americans will die from the disease [68]. One of the precursors of this disease is the presence of adenomatous polyps in the colon. Current medical evidence supports the theory that virtually all colorectal cancers develop from adenomas [81]. If these adenomatous polyps can be located and removed before they become cancerous, then many of these early deaths could be avoided.

Case control studies have shown the benefits of screening for colon cancer [65, 52]. During colorectal screening, the interior of the colon is inspected for the presence of adenomatous polyps. However, not all polyps viewed in the colon are adenomatous. Unfortunately, it is usually difficult or impossible for a doctor using a colonoscope to

discriminate visually between different types of polyps. Because visual discrimination of polyps is so difficult, most doctors remove all polyps and biopsy them, although in many cases the excised polyp was not cancerous and did not need to be removed. It is not desirable to remove a polyp unless it poses a threat to the patient.

Currently, the only clinically validated method of determining the classification of colorectal polyps is through a histological examination of biopsied tissue samples [3]. In this technique, the polyp is removed, and its microscopic structure is examined in order to determine what type of polyp it is. An in vivo method of diagnosing colorectal polyps would reduce the number of biopsies needed. As a consequence of this, costs for colorectal cancer screening would decrease and patient care would be improved. A number of non-invasive techniques have been proposed to enable in vivo diagnosis of polyps. These include such methods as magnifying colonoscopy using dyes, spectroscopy, confocal microscopy, optical coherence tomography, and ultrasonography. All of these techniques require additional equipment, some very expensive, for the diagnostic process. This thesis describes a method to classify polyps in vivo without the need for special equipment or dyes.

During colorectal cancer screening procedures, if the physician observes a polyp in the colon, he typically takes a digital image of the polyp and resects it for biopsy. The image is placed in the patient's records for follow-up screening purposes. We use the information in this image to create an algorithm which will classify the polyp. The diagnosis provided by this algorithm would become available to the physician during the examination so that he will be able to make a more informed decision on whether the polyp is adenomatous and should be removed, or if it is hyperplastic and excision is not required.

Some examples of polyp features that may be of use in classifying the polyp are

the patient's age, sex, and history of previous polyps. These four features are known before the patient's examination. Features that become known during the procedure include the size of the polyp and its location in the colon. In this thesis, size information was known from biopsy data, not from measurements taken during the endoscopic examination. However, size can be estimated in vivo and is an important indicator for the classification of polyps. For these reasons, it was included in the discrimination.

Researchers have attempted to determine what information may be culled from the image of a polyp. They have found a strong correlation between the texture of a polyp, its color, and its probability of malignancy [28, 29, 3, 40, 32, 39, 54]. However, there is no consensus on a method to quantify these features. In this thesis, we will attempt to quantify the texture and color of neoplastic and non-neoplastic polyps so that additional features may be used to classify polyps. When quantifying these features, we will need to take into account the fact that in clinical practice, polyp images are taken from different camera positions, under different lighting conditions, and at different distances between the camera and the polyp. Therefore, features used to classify the observed polyps must be robust under these varying conditions. The features used in this thesis, including radial frequency response and fractal dimension, were chosen for their robustness under these varying conditions.

In our approach, the available polyp images have been split into two sets: a training set for the classifier and a test set. Once the feature vectors were calculated for the training data, they were used to generate the weights for a linear discriminant function. This function was then used to evaluate the algorithm's performance for the series of test images for different size subsets of the feature set.

1.2 History

There is a demand in medicine today for techniques that will allow precise diagnosis and shorten patients' recovery times [6]. A technique known as minimally invasive surgery (MIS) is helping doctor's meet these demands. One method of MIS, endoscopy, involves the use of a flexible tube to inspect the body's internal organs and cavities. The use of endoscopy has many benefits for both the patient and the doctor. Since endoscopes can be inserted through a small incision or natural body opening, they allow surgical procedures to be performed in the least invasive manner possible. This greatly reduces the patient's recovery time and discomfort [50, 6]. Furthermore, endoscopy allows the doctor to get a much better view of a disease in its natural environment than he would have without this technique.

Endoscopy first began in the early 1800s. The first endoscope, an open-tube system using candle-light for illumination, was introduced in 1806. During the 1870s, telescopic tube systems using glass rods and lenses were developed to look deeper into the body. One problem with these systems however was that they were rigid and not able to peer into tortuous tracts, such as the colon [6]. Modern endoscopy began in 1958 with the advent of the fiber-optic endoscope. This was a major improvement over the previous systems. The fiber-optic endoscope was composed of a slim, plastic tube with a lens at one end and a bundle of optical glass fibers to carry the image to an eyepiece. The tubes were coupled with a light source to illuminate the interior of the body [5]. The flexible construction enabled the doctor to gain a much better view of the interior of the patients body than had been allowed by previous systems.

The next breakthrough for endoscopy occurred in 1983 when Welch-Allyn, an instrument maker in New York State, first produced CCD (charge-couple device) endoscopes. Though similar in construction to the old fiberoptic endoscopes, there were several important differences. These new endoscopes had a tiny CCD camera mounted at the instrument's tip connected by wires to the doctor's end of the scope. The CCD consist of a 2D array of Silicon photodetectors which convert optical images to electrical signals. A video processor converts analog electronic signals to digital signals (A/D conversion). However, using red, green, and blue colored optical filters or color CCD technology, these new instruments allowed full color imaging [21, 77]. This new technology also enabled the image to go directly to a computer or video screen [5].

Since fiberscopes had been used successfully for so many years, physicians at first doubted that this new technology would have any clinical use [37]. However, studies have shown that electronic endoscopes can perform at least as well as fiber endoscopes, and in recent years, the performance of the video endoscope has exceeded that of the old fiberscope [37, 66]. The advent of the videoendoscope in endoscopy has provided several important advantages. First, unlike the old fiberscopes, the video endoscope does not easily break after prolonged use. Second, because the doctor is no longer tied to an eyepiece, both the doctor and the patient can view an endoscope procedure on a video monitor, making the procedure easier for both of them. Third, the quality of the images obtained is better than those seen through the traditional fiberscope, and, since they are digital images, different digital image processing techniques may be applied to the images [37]. Although there have been no reported incidents in which anything invisible to the naked eye has been made visible with this technology, image processing may accentuate weak features that would

normally only be visible to experts [20, 21]. Finally, and most importantly, videoendoscopy enables the images to be stored digitally so that a record of patients' examinations may be kept. This enables doctors to store and transmit the images if a referral is necessary. A large database of these images provides better tracking of the patients condition [59]. The combination of high quality images and the accumulation of a large database of such images makes large-scale studies to determine automatically the classification of a colorectal polyp, such as discussed in this thesis, an important new area of research.

1.3 The Problem

The presence of adenomatous polyps can be detected through a number of methods. These include fecal occult blood testing, barium enema in combination with radiography, and endoscopy [81]. However, there are less choices available for polyp diagnosis. The gold standard for polyp diagnosis is through histology. The only method to remove a polyp for biopsy without performing major surgery is through colonoscopy. In this method, the physician uses a video colonoscope to survey the interior of the patients colon. If the physician observes a polyp or other anatomical anomaly, he will take an image of the structure, and if it is a polyp, will resect it. Resected polyps are sent to pathology, and the histological findings are then used to diagnose the polyp. Table 1.1 names and categorizes the types of polyps which occur in the colon [68]. Adenomatous polyps are a category of neoplastic polyp, which also include the carcinomas (cancers). Hyperplastic polyps are a subset of non-neoplastic polyps. Although hyperplastic polyps may rarely (less than 1% of the time) become focuses of adenomatous change, it is assumed that hyperplastic polyps

Table 1.1: Classification of Colorectal Polyps

<table>
<tr><td rowspan="12">Colorectal Polyps</td><td rowspan="4">Neoplastic Mucosal Lesions</td><td rowspan="3">Benign (Adenoma)</td><td>Tubular Adenoma</td></tr>
<tr><td>Tubulovillous Adenoma</td></tr>
<tr><td>Villous Adenoma</td></tr>
<tr><td rowspan="2">Malignant (Carcinoma)</td><td>Carcinoma in situ (intramucosal)</td></tr>
<tr><td>Invasive Carcinoma (through Muscularis Mucosae)</td></tr>
<tr><td rowspan="5">Non-Neoplastic Mucosal Lesions</td><td colspan="2">Normal Epithelium(in a polypoid configuration)</td></tr>
<tr><td colspan="2">Hyperplastic Polyp(Metaplastic Polyp)</td></tr>
<tr><td colspan="2">Juvenile Polyp(Retention Polyp)</td></tr>
<tr><td colspan="2">Peutz-Jeghers Polyp</td></tr>
<tr><td colspan="2">Inflammatory Polyps(Pseudopolyps)
• inflammatory Bowel Disease
• in bacterial infections or amebiasis
• schistomiasis
• colitus cystica profunda</td></tr>
<tr><td rowspan="5">Submucosal Lesions</td><td colspan="2">Pneumatosis Cystoides Intestinalis</td></tr>
<tr><td colspan="2">Lymphoid Polyps (benign and malignant)</td></tr>
<tr><td colspan="2">Lipomas</td></tr>
<tr><td colspan="2">Carcinoids</td></tr>
<tr><td colspan="2">Metastatic Neoplasms</td></tr>
<tr><td colspan="3">Other Rare Lesions</td></tr>
</table>

will not become malignant [3]. For the purpose of this research, we are only attempting to classify these two types because, together, they account for 80%-90% of all polyps [81].

There are a number of other methods in development which would potentially allow in vivo polyp diagnosis during endoscopy. Current diagnostic research falls into three categories: spectroscopy (including fluorescence and Raman scattering), imaging (including optical tomography and confocal microscopy), and ultrasonography. In the method of optical spectroscopy, tissue is probed using light delivered by optical fibers inserted through the instrument channel of the endoscope. The measured optical response provides information about the local tissue biochemistry and morphology [67, 34]. This information can

be used to diagnose pre-malignancies with good accuracy. Numerous papers have been written on the potential for flourescence spectroscopy to distinguish between normal and potentially malignant colorectal tissue [33, 13, 47, 48, 82, 7]. Frank used Raman techniques to differentiate between normal and diseased human breast tissue [19].

Two other techniques being examined for in vivo polyp diagnosis are optical coherence tomography [70, 9] and ultrasonography [53, 10]. Both of these techniques allow high-resolution imaging of tissue microstructure. Optical coherence tomography works "by focusing an optical beam onto the tissue, the echo time delay of light reflected from the internal microstructure at different depths is measured by interferometry. Image information is obtained by performing repeated axial measurements at different transverse positions as the optical beam is scanned across the tissue. The resulting data constitute a two-dimensional map of the intensity of light backscattering from internal architectural morphology and cellular structures in the tissue." [70] Ultrasonography uses a similiar method to obtain images of the tissue's microstructure except acoustic waves instead of infrared lightwaves are used [70]. Lastly, there is a technique known as confocal microscopy. This technique employs optical sectioning to image through optically thick samples to observe the microstructure of an area.

All the methods described above are based on attaching additional pieces of equipment to the traditional endoscope or using special equipment that is passed through the instrument channel of the colonoscope. This equipment is not normally used during colon cancer screening. A method which utilized current technology and took very little or no training to operate would be very beneficial, especially if it could work for the physician in real-time, providing the doctor with immediate feedback.

1.4 Proposed Approach

Endoscopists are working toward the goal of histological diagnosis during endoscopy [40]. Results so far have been mixed. Besides the techniques mentioned above, the efforts of researchers have moved in two directions. These are the enhancement of the ability of the physician to make in vivo diagnosis and the development of an automatic classification technique.

Two classes techniques have been developed to attempt to enhance the ability of doctors to make in vivo diagnosis. In one class of techniques, image enhancement algorithms are applied to the available digital endoscopic images in order to enhance those features which doctors feel allow them to make diagnoses. This has been used to make detecting cancers on the bronchus surface easier [55], to accentuate the appearance of peptic ulcers [62], and to enhance mucosal surface structure [20]. However, despite the considerable amount of work that has been done in this area, image processing techniques have not been found to have any effect on clinical diagnosis [69, 11, 21]. The other class of techniques to enhance images involves the use of more expensive equipment. Doctors have begun to use magnifying endoscopes and dyes in investigations. The dyes are used to make the texture of polyps more clearly visible, and the magnifying endoscope is used to look more closely at the polyp's surface structure [40]. These techniques have met with a fair degree of success.

Doctors also have attempted to discover if pattern recognition techniques could be applied to endoscopic images in order to enable automatic polyp diagnosis. One study by Kohsen compared the line structures of images of gastric polyps, carcinoma, and mucosa and claimed to see a difference–though a differential diagnosis could not be made [38].

More efficient techniques have been proposed by Cross and Verhest. These techniques each use multiple features in attempting to classify polyps. Cross investigated the relationship among different polyp types and the characteristics of patient's age and sex, size and form factor of the polyp, and fractal dimension of the image of the polyp's surface. He found that fractal dimension was useful in distinguishing between different polyp types [15]. Verhest distinguished between different types of polyps based on different morphonuclear image parameters [80]. These studies, though promising, did not attempt to distinguish among types of polyps in vivo. In each case, images of ex vivo samples of stained and magnified tissue were used in the discrimination.

It is the hypothesis of this thesis that pattern recognition techniques applied to biopsy samples and morphonuclear images can also be applied to images taken of polyps in vivo. Unlike the previous research in this area, the images used in this thesis were not taken in a controlled environment. The features in the discriminant must be able to account for different viewpoints of the polyp, different sources of illumination, and different imaging distances. Therefore, for this research, we developed a method to extract a robust set of features (metrics) from the images of polyps acquired in vivo, devised an algorithm to evaluate a polyp based on these metrics, and evaluated the performance of the algorithm. The features under consideration are measures of size, location, color, texture, and shape of the polyp, as well as the age of the patient. To accomplish this, first, the endoscopic images were processed to mark areas of glare. Then, the image was processed to accentuate the features of interest (in our case, texture and color). Features were calculated from manually selected regions of interest in the processed images. Finally, these features were used in a linear discriminant function to perform an objective automatic classification of the polyp.

Previous research has focused on evaluating these classes of features in isolation. In this thesis, features from all the classes were evaluated in order to determine the optimal reduced feature set.

1.5 Contributions and Benefits

The objective of this thesis was to create a diagnostic tool that could be used to classify colorectal polyps in vivo. As mentioned previously, since there is no current non-invasive technique to do this, many unnecessary polyp excisions and biopsies are performed. The cumulative costs of these procedures are rapidly rising as the population of the United States ages. The American Cancer Society has recommended that all persons past the age of 50 undergo screening sigmoidoscopy every 3 to 5 years [45]. It has been estimated that 60 million people past the age of 50 would be eligible for screening every 5 years [60]. If only 15% of patients were found to have hyperplastic polyps that needed biopsy for diagnosis or subsequent colonoscopy, the screening cost would exceed $100 million [3]. A visual determination to classify polyps would not only help lower these costs, it would also raise the quality of patient care by preventing the need for unnecessary medical procedures.

A secondary objective of this project was to create a tool that could be incorporated into a doctor's normal procedures during colorectal screening with a minimum of additional time taken during the procedure and a minimum of additional software required. The work in this thesis represents an important first step in the development of such a tool. For this reason, the data analyzed by the algorithm consists of the images taken taken by a gastrointestinal endoscopist during standard colonoscopy sessions. Also, unlike the dif-

ferent techniques such as spectroscopy, ultrasonography, and so on, doctors could benefit from this procedure without needing to obtain additional hardware.

Finally, this algorithm could be executed in real-time system with a minimum amount of additional work to be done by the examining physician or by the physician's assistant. This would provide the doctor with immediate feedback regarding the classification of an observed polyp. This will give the doctor an additional piece of information to aid him in gauging a polyp's potential malignance. Hopefully, this technique will give doctors enough information to make a diagnosis on the polyp in vivo, but, even if it does not, it may provide a useful way to determine if some other non-invasive diagnostic method should be applied (such as spectroscopy, optical coherence tomography, et al).

1.6 Organization

The organization of this thesis is as follows. In chapter 2, we explore the different features which may be used to classify the malignancy of a polyp and how they may be extracted from the available data. In chapter 3, we discuss decision theory and how the method of linear discriminant analysis can be used to differentiate between two disparate groups of data given a number of observations. In chapter 4, the ideas from chapters 2 and 3 are combined and used to classify polyps from endoscopic images based on the features discussed in chapter 3. The performance of the algorithm is evaluated for different combinations of features. Chapter 5 offers suggestions for future work and summarizes the work contained in this thesis.

Chapter 2

Features and Feature Extraction

2.1 Overview of all Features

A polyp is defined as "any tissue protrusion above the mucosal surface. Polyps may assume varying size and shapes. A polyp can be described by the texture of its mucosal surface, color, presence of a stalk, ulcerations, or bleeding." [81] Many researchers have investigated the characteristics of polyps and how these characteristics may be used to identify the type of polyp being observed. The two most widely studied polyps are also the most common: adenomatous polyps which are neoplastic and the most common form of non-neoplastic polyp, the hyperplastic polyp. Together, these two types make up more than 80% of all polyps found during endoscopic examination [81]. In the following sections, we discuss the correlation of different features with the potential malignance of colorectal polyps. We also discuss methods of quantifying these features.

Table 2.1: Non-image Based Features Considered in the Discrimination

FEATURE CLASS	FEATURE DESCRIPTION
Age	Patient's Age
Size	Volume of Polyp
Location	Location Found in the Colon

2.2 Features not Gained from the Images

2.2.1 Overview

Several examples of features of colorectal polyps that researchers have investigated are the sex of the patient, the patient's age, the location of the polyp in the patient's colon, and the size of the polyp. The correlation between the sex of the patient and the presence of adenomatous polyps is not detailed here because adenoma polyp occurrence is roughly the same in men and women [81]. Some researchers have found that these features depend on the geographic location of the patient. A study by Cronstedt investigating adenomatous polyp frequency in different areas of Sweden found that there were regional differences in the age of patients who developed adenomas and in the distribution of adenomatous polyps in the colon [14]. If these features are part of a classifier, the operator should ensure that the training data and the test data come from the same geographic area. Accounting for possible geographic differences and different types of polyps is beyond the scope of this thesis. The features considered in this section are shown in Table 2.1.

2.2.2 Age

It is widely believed that the frequency of adenomatous polyps increases with age [81]. However, when Cross attempted to use age information in a discriminant function, he found that age added no new information to his discriminant [15]. Therefore, the exact correlation between age and the frequency of adenomatous polyps is still inconclusive. Is it the case that older people more likely to have polyps with an equal chance of adenomatous or hyperplastic types? Or is it the case that polyps found in older people are more likely to be adenomatous? In order to see if age provided any discriminatory power to our discriminant, age was included in the discrimination analysis of this thesis. As a feature, the age was used directly, i.e. if a person was 62 years old, 62 was used as a feature for his polyp. If older people are more likely to possess adenomatous polyps, then a larger value for age should bias the discriminant towards choosing adenoma as the diagnosis.

2.2.3 Size

Doctors have known for many years that there is a link between the size of a polyp and the likelihood of it containing pre-malignant tissue. In research by Kronberg, researchers found that of all stalked polyps greater than 5mm in size 82% were adenomas [39]. Norfleet and Iida also found a link between size and potential malignancy [54, 28]. Luk reports that of all polyps, 75% are adenomatous, and of polyps less 5mm, 50% are adenomas, which indicates that polyps larger than 5mm in size were more likely to be adenomatous than hyperplastic [81]. As late as 1995, Jaramillo reported a link between the probability of a polyp being potentially malignant and its size [32]. Obviously, size is less effective in

distinguishing between small adenomas and hyperplastic polyps. However, the size feature does provide an easy way to separate out those large polyps which would be excised by the physician regardless of their classification.

Research has been done on the effectiveness of estimating polyp size in vivo. Usually the physician estimates the size of a polyp by comparing it with the known opening width of a set of tweezers passed through the instrument channel of the colonoscope. This is accomplished by putting both the tweezers and the polyp in the field of view and estimating the size of the polyp by eye. Although some research had shown that polyps were estimated to be consistently smaller than their true size [49], other research has shown that the size of objects can be measured accurately with an endoscope [25, 77]. Moreover, Vakil made the technique more accurate by correcting for the distortion of the lens of the colonoscope [77]. The technique for correcting for the lens's distortion is discussed further under shape measurements. Since it is possible to estimate polyp size in vivo, we decided to include the feature in the discriminant to observe its effect.

Unfortunately, in the data available for this thesis, size was not estimated during the examination. It only became available post extraction, during the biopsy procedure. Due to this, error entered into the size measurements from two sources. First, during polypectomy, the doctor tends to remove some of the tissue around the polyp in order to verify that the polyp has not spread into the surrounding area. Therefore, measured size of the polyp may be larger than its actual size. Second, sometimes polyps break apart during resection and only pieces are available during biopsy. The aggregate size of the reconstructed polyp may not be completely accurate. Nonetheless, we decided to use the total volume of all the pieces of the polyp (in mm^3) as a feature. Greater volume should

Table 2.2: Anatomic Distribution of Colonic Adenomas

Location	Colonoscopy	Autopsy (all adenomas)	Autopsy (adenomas>1cm)
Ascending	10%	30%	15%
Transverse	10%	20%	15%
Descending	30%	15%	25%
Sigmoid	45%	15%	35%
Rectum	5%	20%	10%

indicate a greater chance of being an adenoma.

2.2.4 Location

The exact correlation between a polyp's location in the colon and its potential malignance is inconclusive. Most of the research has shown that a majority of polyps have been found in the left side of the colon (the proximal end of the colon is considered to be the end of the colon nearest the small intestine), though this changes with age. Hyperplastic polyps are usually found in the rectosigmoid area. Common wisdom says that this occurs because polyps are more easily accessible in this area during colonoscopy and sigmoidoscopy (and hence more easily seen and reported on) [81].

As table 2.2 [81] shows, autopsy results demonstrate an even spread of adenomatous polyps throughout the colon; which seems to disprove the theory that adenomatous polyps are more prevalent in one area than another [81]. Newer research does seems to indicate that there is some correlation between the location of a polyp and the probability that it is an adenoma. Norfleet reported that hyperplastic polyps were located closer to the rectum than adenomas. Axelrad reported that of all the polyps in his study that most hyperplastic polyps were found in the rectum and sigmoid. Adenomas were most likely to

be seen in the proximal colon and the splenic flexure [3]. Another study found that 60% to 79% of all polyps near the splenic flexure were neoplastic, compared with 8% to 28% elsewhere [32]. From these results, one may observe that there is a relationship between polyp location and its classification, but the exact relationship is still undetermined.

Unfortunately, it is generally very difficult to estimate the location of a polyp during colonoscopy. The distinction between different sections of the colon is not always readily apparent due to the twists and folds of the large intestine. Often times, the doctor must make an educated guess as to a polyp's location. By necessity, this type of measurement will be imprecise. During an autopsy, this error does not arise, since the whole colon can be removed and immobilized in clamps. In the pathology data available to us, the doctor reported the location of the polyp. The different regions of the colon were labeled as noted in Table 2.3 and this was used as the location feature. For example, if a polyp was found in the rectum, it was assigned the number 15 as a feature.

2.3 Features Calculated from the Images

2.3.1 Overview

Once all features are extracted from the images of the polyps, the conditions under which the image was acquired must be examined. The image of a particular object may change quite a bit if viewed from different attitudes or different distances from the camera to the object or even under different lighting conditions. In many pattern recognition algorithms, one or more of these factors may be considered to be constant in the images. This is not

Table 2.3: Major Areas of the Colon and Numbering Scheme

Name of Area	Assigned Number
PROXIMAL ASCENDING	1
MID ASCENDING	2
DISTAL ASCENDING	3
HEPATIC FLEXURE	4
PROXIMAL TRANSVERSE	5
MID TRANSVERSE	6
DISTAL TRANSVERSE	7
SPLENIC FLEXURE	8
PROXIMAL DESCENDING	9
MID DESCENDING	10
DISTAL DESCENDING	11
PROXIMAL SIGMOID	12
MID SIGMOID	13
DISTAL SIGMOID	14
RECTUM	15

the case with the polyp images.

The images were acquired under a variety of lighting conditions, distances, and polyp poses. Since our features of texture and color do not vary based on the pose of the polyp, pose does not present a problem to us. However, the conditions of lighting and distance from polyp to camera do affect our measurements. Distance is a problem because many times the surface details of the polyp can only be seen within a certain range. This optimal viewing distance depends on the optics of the endoscope, but it is generally about 1 cm. These details will become blurred and disappear if the image is acquired outside that range. Since the apparent size of features will change depending on viewing distance, this implies that scale will be a problem.

Changing lighting from one image to the next is also a problem. Lighting changes may occur because the light source is different on different endoscopic cameras. This

changes the amount of energy reflected by the surface under inspection which in turn changes the amount of energy absorbed by the CCD in the camera. This alters the value recorded for the pixel value in the image. This means that from one image to another that the pixel values will be altered by some non-linear scale, which is not known.

Another problem arises from specular reflection in the image. Specular reflection (or glare) is produced when the light from the camera is reflected by mucous or some other substance coating the sides of the colon. When the CCD is saturated by a region reflecting too much light, the value recorded is its highest value which appears as white in the image. Also, unsaturated pixels adjacent to the saturated pixel may be affected by "blooming"– spill off counts. Areas of glare in the image contain no information about the polyp's surface characteristics, making it impossible to calculate the value of a feature in this area. For this thesis, an algorithm was developed to find the regions of the image affected by glare. The glare detection algorithm defines an image, MAP, of the same size as the input image. Each pixel in MAP corresponds to a pixel in the input image. MAP's pixels have the value 1 for those pixels in the input image affected by glare and 0 for those pixels not affected by glare. The MAP image was used to indicate what pixels should be involved in the feature calculations. If glare affected the calculation of a particular feature, the change in the algorithm to deal with the glare is noted below. Generally, this meant that that pixel was excluded from the feature calculation. The algorithm used to generate the MAP image is described in Chapter 4.

2.3.2 Texture Features

In this thesis, we attempt to distinguish between two types of polyps: adenomatous polyps and hyperplastic polyps. These polyps have markedly different morphological structures which is how they are differentiated histologically under microscopic viewing. These differences have been highlighted in several electron microscope studies [1, 2]. Of course, a difference in microscopic structure does not necessarily imply a useful difference in the macroscopic structure visible to the camera. Fortunately, studies have found that visible surface structure under magnifying endoscopy may be used as a useful discriminant in separating different classes of polyps. These studies have shown that hyperplastic polyps have a pattern of dots of generally less than 100μm in size and that adenomatous polyps do not [3, 40, 81, 2]. The features on adenomatous polyps could be over six times as large [1]. The appearance of adenomatous polyps ranges from a nodular (grooved) surface to a granular surface, depending on the degree of villous structure [28, 29]. In these studies, the researchers used high-magnification endoscopes with dye to observe the fine details of the surface structure. In order to pick out specific details, 100x magnification was needed. However, differences between differently textured polyps could still be appreciated at normal magnifications using dye to improve contrast [40, 3]. Compared with stereomicroscopic diagnosis, Kudo identified 81.5% of all polyps correctly utilizing a magnifying endoscope and dye. Kudo was able to sketch the gross surface structure of the major types of colorectal polyps [40]. He found that the exophytic (rising above the surface of the colon) hyperplastic polyps had dots on their surface and adenomatous polyps had a series of grooves.

In the polyp images obtained for this thesis, we observed that the characteristic

Table 2.4: Texture Features Considered in the Discrimination

FEATURE CLASS	FEATURE DESCRIPTION
Texture	Fractal Dimension
Texture	Radial Frequency Bins
Texture	Normal Dispersion
Texture	Textural Edgeness-Sobel
Texture	Textural Edgeness-Laplacian
Texture	Histogram-Dispersion
Texture	Histogram-Variance
Texture	Histogram-Energy
Texture	Histogram-Skewness
Texture	Histogram-Kurtosis
Texture	Histogram-Entropy

surface structures of both the adenomatous polyps and the hyperplastic polyps were at the limit of the camera's resolution. Typically, endoscopic cameras may distinguish features as small as 100μm. However, the hyperplastic surface structure tended to be smaller and harder to see than the gross surface structure of the adenomatous polyps. This means that the hyperplastic polyp had no visible features which were characteristic of all the images. On the other hand, adenomatous polyps had a grooved or villous structure that was readily seen in many of the images. Examples of these types of surfaces are shown in Figure 2.1 and Figure 2.2. For this reason, the assumption was made that any calculation of texture would need to take into account the limits of the resolution, and it could be assumed that the hyperplastic polyp would appear smoother than the adenomatous polyps. Therefore, the texture measures attempt to characterize the "roughness" of the polyp's surface. The features considered in the texture analysis are listed in Table 2.4.

Figure 2.1: Tubular Adenoma

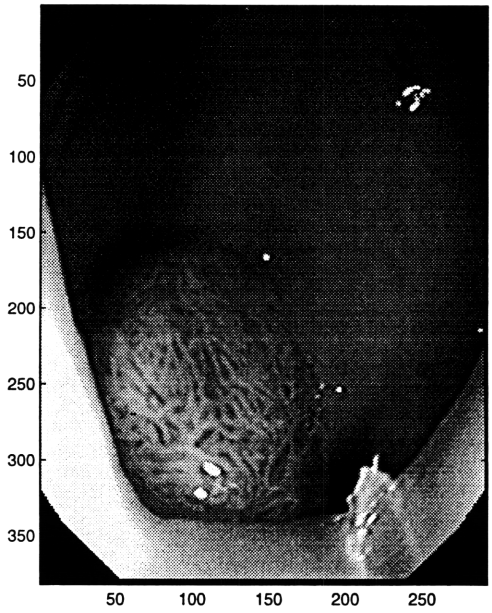

Fractal Dimension

For disordered surfaces (surfaces with no regular pattern or direction), fractal dimension is a useful measure to discriminate one type of surface from another [61]. Research has shown that fractal dimension of a surface matches well with our perception of roughness. In general, as the computed fractal dimension of a surface increases, a human observer will perceive it as becoming rougher [58].

The fractal dimension of a surface has been used to detect edges and to classify liver images [12], to evaluate the topography of Oregon [26], to distinguish between colorectal polyp tissue [15], to analyze cervical cells [46], to find tanks [23], and to quantify chaos [71]. In Cross's study, fractal dimension was found to be a useful metric in separating different types of polyps [15]. However, this evaluation was done under very controlled

Figure 2.2: Villous Adenoma

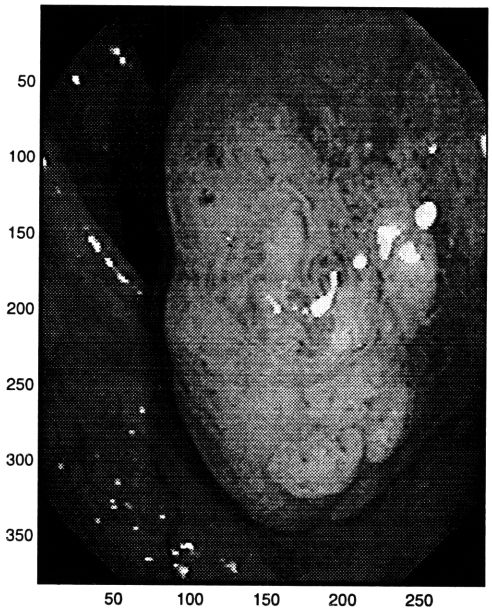

conditions (the images were of stained tissue under a microscope) so it is unclear whether fractal dimension will be as useful when applied in this study. The calculation of fractal dimension has been found to be robust under a range of conditions for noise, variable contrast, and brightness [18]. This is an important quality because the images available in this study have variable brightness and contrast.

In image analysis, relationships have been found among fractal dimension, scaling, power spectrum, area size, and intensity differences [12]. A number of techniques to estimate fractal dimension have been devised in order to take advantage of these relationships. Pentland used the power spectrum of an image to estimate its fractal dimension [58]. Peleg used the size of the intensity surface area at different scales [56]. Gagnepain developed the reticular cell counting method [22], Dubuc used a variation method, [17], and

Schepers investigated relative dispersion, correlation, rescaled range, and Fourier analysis [64]. Peli described the covering blanket approach [57].

Care should be taken in choosing a method to calculate the fractal dimension for a particular problem. Research has found that the calculation of fractal dimension using box counting and variation may not be very accurate in some cases [27]. A researcher concerned with the true fractal dimension of a surface may not be satisfied with the results obtained using these techniques. However, it has been found that estimates of fractal dimension for these techniques do vary monotonically with the true fractal dimension under consideration. Therefore, the results may be useful for surface characterization. In this thesis, we are examining the relative roughness of surfaces and so we are not concerned about a rigorous evaluation of the fractal dimension of a surface; a general estimate of the roughness of a surface should be sufficient. The algorithm described below was tested on a series of images. The first image began as a flat surface and later images in the series had increasing amounts of noise added to them. The calculated fractal dimension versus the magnitude of the noise is shown in Figure 2.3. The behavior is monotonic.

The technique we employed is based upon the reticular cell counting method described in Rao [61]. The input to the algorithm is a section of an $M \times N$ region of the input image specified by the operator to lie on the polyp's surface. Given the input image, $x(n_1, n_2)$ specified to have Q gray levels, where $n_1 = 1, 2, ..., M$ and $n_2 = 1, 2, ..., N$, we can calculate the surface's fractal dimension. The input image has dimensions $M \times N \times Q$. We want to put the image into a cubic 3D space of dimensions $P \times P \times P$. To perform this transformation, we have to choose a value for P. This can be done by calculating $P = min(M, N)$, where P is the minimum dimension of the image. Then, we resample

Figure 2.3: Increasing Fractal Dimension with Increasing Noise

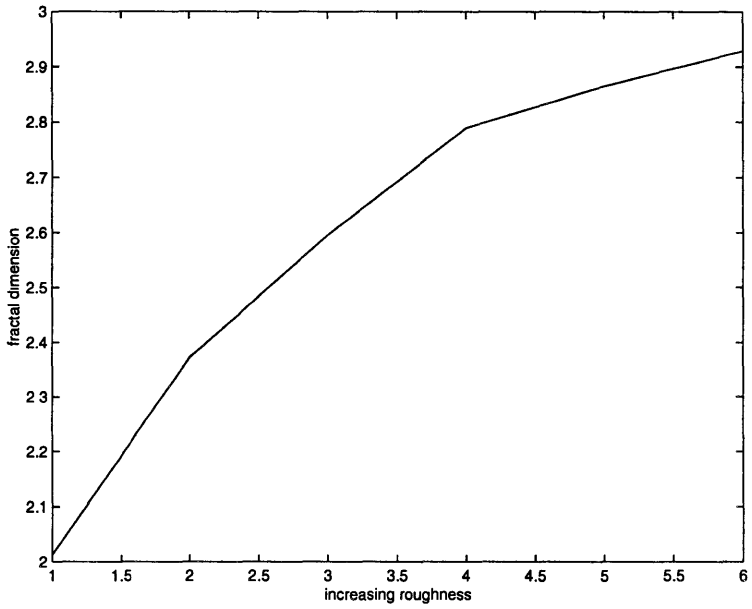

the surface and the surface's gray levels so that it becomes a region of size $P \times P$ with P gray levels. The image now resides in a cubic space. We now define a cubic array, C, of dimensions $P \times P \times P$. In C, there are P^3 subcubes that correspond to every 3D position in the cubic space into which a gray level could be mapped. C has zeros in all these subcubes except for those which correspond to a gray level which the discrete pixel points of $x(n_1, n_2)$ have been mapped. These subcubes contain ones.

At this point, the cubic array, C, contains a discrete set of points. In order to find the fractal dimension, we need to find the surface which connects these discrete points. To put this another way, it is necessary to find the subcubes of C through which the surface connecting the points from the resampled image passes through. The method used in this thesis proceeds as follows. We begin processing in the top left corner of the

image. This corresponds to position $x(1,1)$ in the resampled image. The C array has a 1 in position (1,1,N_1) representing the pixel's gray level. We desire to connect this position with those below it and to its right. These positions correspond to $x(2,1)$ and $x(1,2)$ in the resampled image with ones in C at positions (2,1,N_2) and (1,2,N_3), respectively. N_1, N_2, and N_3 are integer numbers between 1 and P representing the different levels into which a gray level from x(n_1,n_2) could be mapped. We wish to connect these discrete points in C. The following two rules are used to connect the discrete points. To connect a point with a point to its right, we fill all the points in C between (1,2,N_1) and (1,2,N_3) with ones. To connect a point with the point below it, we fill all the points in C between (2,1,N_1) and (2,1,N_2) with ones. We use these two rules to process every point in C. In the end, all the subcubes which the surface passes through should be filled with a one; all other subcubes should contain zeros. We can add up all the subcubes that have a one in them, and we will call this result, P_1.

After this result is obtained for the cube of side P, we repeat the process for a resampled cube of side length $\frac{2}{3}$P. We continue this process until we have two vectors of length 4. One is defined as P=$[P_1, P_2, P_3, P_4]$ which contains the number of subcubes which the surface passes through on each iteration. The other, R, is defined as R=$[1, \frac{3}{2}, (\frac{3}{2})^2, (\frac{3}{2})^3]$ which contains the length of the side of a single subcube for a particular iteration, where the size of a subcube on the first iteration has been normalized to 1. We can write the following relation [61]:

$$N(\lambda) = \lambda^{-fd} \tag{2.1}$$

where $N(\lambda)$ is the number of subcubes through which a surface passes for a particular cube

edge size λ. fd is the fractal dimension of the surface. By taking the log of this relationship, we can derive

$$fd = -\frac{\log N(\lambda)}{\log \lambda} \tag{2.2}$$

This gives us a way to to measure the fractal dimension of a surface. By fitting a line through the points given in the P and R vectors, we will find that the fractal dimension is equal to the slope. We can write a vector equation to relate the two sets of points in the form of $Ax = b$ where $x = [m, b]$, m is the slope of the line and b is the intercept. A and b are defined below.

$$A = \begin{bmatrix} \log(R_1) & 1 \\ \log(R_2) & 1 \\ \log(R_3) & 1 \\ \log(R_4) & 1 \end{bmatrix} \tag{2.3}$$

and

$$b = \begin{bmatrix} \log(P_1) \\ \log(P_2) \\ \log(P_3) \\ \log(P_4) \end{bmatrix} \tag{2.4}$$

Then, x can be solved for using

$$x = (A^T A)^{-1} A^T b \tag{2.5}$$

where $m = x(1)$. Fractal Dimension is equal to $-m$.

For every input image, the fractal dimension was calculated. Since the surface of an adenomatous polyp is assumed to be rougher than that of a hyperplastic polyp, the

calculated fractal dimension of an adenomatous polyp should be higher.

Radial Frequency Response

All the texture information in an image can be captured by its frequency response. The frequency response can be used to derive various measures that will give us information about the texture being observed. One of these measures is called the radial frequency response of the signal. In this measure, the frequency response is separated into radial bins emanating out from the origin of the signal in the frequency plane. The total signal power falling into each bin can be calculated and used as a feature [4]. Then, each bin can be normalized by the sum of the energy that fell into all the bins. This will provide the percentage of the signal energy that fell into each bin. Another piece of information that can be taken from the frequency response is the directionality of the texture. The polyp texture was not observed to have a dominant direction so this property of the frequency response was not explored.

Three types of textures were observed in the images. The first two were found on the adenomatous polyps, and they corresponded to either a granular or a nodular appearance. The third texture was found on the hyperplastic polyps, and it corresponded to a smooth appearance. A general rule of thumb when evaluating signals is that the more changes that occur in a time signal (or in a spatial signal such as an image), the greater the percentage of the signal energy which will fall into the higher frequency components. This means that the rougher images will have a higher percentage of their energy falling into the bins corresponding to high frequency and the smooth images will have more energy falling into the low frequency bins. This is the behavior we hope to capture. A description of how

the radial frequency response is calculated is provided below.

Given a discrete input signal, $x(n_1, n_2)$, where $n_1 = 1, 2, ..., M$ and $n_2 = 1, 2, ..., N$, we can use the Fourier transform to return $X(\omega_1, \omega_2)$.

$$X(\omega_1, \omega_2) = FFT_{P \times P}(x(n_1, n_2)) \tag{2.6}$$

where, for simplicity, the frequency response has been made square by setting $P = max(M, N)$. The DT frequency response of the two-dimensional signal runs from $-\pi$ to $+\pi$ in ω_1 and from $-\pi$ to $+\pi$ in ω_2 in P steps. Then, the dc response may be shifted to the center of the spectrum by setting

$$X_1(\omega_1, \omega_2) = X(\omega_1 - \pi, \omega_1 - \pi) \tag{2.7}$$

Once the signal has been shifted, we know that the DC (zero frequency) portion of the signal lies at the coordinate $(\frac{(P+1)}{2}, \frac{(P+1)}{2})$ in the matrix. We set this component to 0 in order to prevent a DC bias from effecting our results. This DC coordinate will be the origin for our radial frequency response. We now want to define a series of disks radiating out from that point. Each of these disks will correspond to a particular set of radially separated frequencies, the frequency "bins". B will be defined to be the number of bins.

Before we can sum the percentage of the signal that falls into each bin, we must first find the power spectrum of the signal. This is defined as the following value:

$$X_p(\omega_1, \omega_2) = |X_1(\omega_1, \omega_2)|^2 \tag{2.8}$$

Since we know what frequency corresponds to which pixels of the transformed signal, we

can use pixel coordinates to separate the frequencies. The set of radii to do this can be defined using the following relationship:

$$b_i = (P/2)/B * i \tag{2.9}$$

where i=0,1,...,B. Using these radii, we can sum up the pixels which belong to each disk using the following equation:

$$bin_j = \sum_{k_1=1}^{P} \sum_{k_2=1}^{P} X_2(k_1, k_2) \tag{2.10}$$

where

$$X_2(k_1, k_2) = \begin{cases} X_p(k_1, k_2) & \text{for } b_j < ((k_1 - \frac{(P+1)}{2})^2 + (k_2 - \frac{(P+1)}{2})^2)^{(\frac{1}{2})} < b_{j+1} \\ 0 & \text{elsewhere} \end{cases} \tag{2.11}$$

We can find the percentage of the signal power which fell into each band by using

$$\widehat{bin_j} = \frac{bin_j}{\sum_{i=1}^{nbins} bin_i}, \tag{2.12}$$

where $j = 1, 2, 3, ..., B$. The percentage of energy that fell into each bin may be used as a feature in the feature vector. Rougher images (corresponding to regions taken from adenomatous polyps) will have a greater percentage of their energy contained in the bins corresponding to the upper frequency bands.

Textural Edgeness

One way of measuring the roughness of an image, is to measure the average edge strength across the image [24]. A rougher image will have more edges and, except in pathological cases, a higher average edge strength. One way of finding the edges in an image is to convolve it with a derivative operator over the image. The output is the edge strength at every pixel in the image. Those pixels whose calculation were effected by glare must be discarded.

Given an input signal $x(n_1, n_2)$ where $n_1 = 1, 2, ..., M$ and $n_2 = 1, 2, ..., N$, two different methods were used to estimate the strength of the edges across the image. The first method uses Sobel's edge masks, defined as

$$S_x = \begin{bmatrix} -1 & 0 & 1 \\ -2 & 0 & 2 \\ -1 & 0 & 1 \end{bmatrix} \tag{2.13}$$

which will detect the vertical edges in the image and

$$S_y = \begin{bmatrix} 1 & 2 & 1 \\ 0 & 0 & 0 \\ -1 & -2 & -1 \end{bmatrix} \tag{2.14}$$

which will find the horizontal edges in the image.

These masks may be convolved with the input image, $x(n_1, n_2)$, to obtain an

output edge image, (where * denotes convolution)

$$OS_x = x(n_1, n_2) * Sx \tag{2.15}$$

$$OS_y = x(n_1, n_2) * Sy \tag{2.16}$$

These two edge images can be combined to demonstrate the total edge strength at each pixel.

$$Edge(n_1, n_2) = (OS_x^2(n_1, n_2) + OS_y^2(n_1, n_2))^{\frac{1}{2}}, \forall n_1, n_2 \tag{2.17}$$

where $Edge(n_1, n_2)$ contains the edge strength at each pixel. Normally, we could just take the sum of all the values in this image and then divide by the total number of pixels in order to obtain the average edge strength. However, we must still take into account the affect of glare in the image.

In order to define the pixels effected by glare, we will need to define another matrix, the identity matrix E, which has the same region of support as the sobel masks used for calculation.

$$E = \begin{bmatrix} 1 & 1 & 1 \\ 1 & 1 & 1 \\ 1 & 1 & 1 \end{bmatrix} \tag{2.18}$$

We can then state

$$EDGE_{map}(n_1,n_2)=\text{MAP}(n_1,n_2)*\text{E} \tag{2.19}$$

All the non-zero pixels of $EDGE_{map}(n_1,n_2)$ will denote pixels that are effected by glare.

We will now define another matrix,

$$\text{MAP2}(n_1,n_2) = \begin{cases} 1 & \text{if } EDGE_{map}(n_1, n_2) = 0 \\ 0 & \text{elsewhere} \end{cases} \tag{2.20}$$

This provides a matrix that has zeros where $EDGE_{map}$ is effected by glare and ones elsewhere. Now, it is possible to column stack $Edge(n_1, n_2)$ and $\text{MAP2}(n_1,n_2)$. The final average edge value may be found by

$$SOBEL_{aes} = \frac{Edge^T * \text{MAP2}}{MN - \sum_{n_1=1}^{M} \sum_{n_2=1}^{N} \text{MAP2}(n_1, n_2)} \tag{2.21}$$

For completeness, a second method was used to calculate the edge strength at each pixel. The Laplacian, a second derivative operator, is defined by

$$L2 = \begin{bmatrix} 1 & 4 & 1 \\ 4 & -20 & 4 \\ 1 & 4 & 1 \end{bmatrix} \tag{2.22}$$

Then, using an argument similar to the one detailed above for the SOBEL edge masks one may arrive at another estimate of the average edge strength in the image, LAP_{aes}.

Histogram techniques

Another way to evaluate the distribution of pixels in an image is through the histogram technique. These measurements require that one first builds a probability function for the pixel distribution in the image. The following algorithm may be used to do that.

Suppose the input signal $x(n_1, n_2)$ where $n_1 = 1, 2, ..., M$ and $n_2 = 1, 2, ..., N$ has L gray levels g_i, where $i = 0, 1, 2, ..., L-1$ with probability density, $p_u(g_i)$. g_{L-1} is the highest pixel value that is not associated with glare. The probability density can be estimated from, $h(g_i)$, where $h(g_i)$ is the number of pixels with gray level value g_i. The probability density function is given by [31]:

$$p_u(g_i) = \frac{h(g_i)}{\sum_{i=0}^{L-1} h(g_i)} \tag{2.23}$$

where $i = 0, 1, 2, ..., L-1$. One can then evaluate the characteristics of this array in order to get information about the distribution of the pixels in the input image. For reference, m_1 is the mean of the distribution defined as

$$m_1 = E[u] = \sum_{i=0}^{L-1} g_i p_u(g_i) \tag{2.24}$$

Dispersion is a measure of the absolute spread of values about the mean. For a low value of dispersion, the pixels are clustered close to the mean [31]. (The image will be smoother.)

$$\text{dispersion} = \sum_{i=0}^{L-1} |g_i - m_1| p_u(g_i) \tag{2.25}$$

A measure of variance carries information about the contrast of the image. It describes the spread of the data so a high variance image will have high contrast. The image will tend

to be rougher for higher values [31, 75].

$$\text{variance} = \sum_{i=0}^{L-1}(g_i - m_1)^2 p_u(g_i) \tag{2.26}$$

The energy value has a maximum of 1 for an image with a constant value and gets smaller as the pixel values are distributed across more gray levels. If the energy is high, the number of gray levels is few [75].

$$\text{energy} = \sum_{i=0}^{L-1}(p_u(g_i))^2 \tag{2.27}$$

Skewness measures the asymmetry about the mean in the gray-level distribution [31].

$$\text{skewness} = \sum_{i=0}^{L-1}(g_i - m_1)^3 p_u(g_i) \tag{2.28}$$

Kurtosis is defined as [31]

$$\text{kurtosis} = \sum_{i=0}^{L-1}(g_i - m_1)^4 p_u(g_i) - 3 \tag{2.29}$$

As the pixel values in the image are distributed among more gray levels, the entropy increases. Entropy varies inversely with energy [75].

$$\text{entropy} = -\sum_{i=0}^{L-1} p_u(g_i) log_2(p_u(g_i)) \text{ bits} \tag{2.30}$$

These values were calculated for each image and used as inputs to the discriminant function. In general humans may appreciate the first and second order statistics of data. However,

Figure 2.4: Calculation of Surface Normals

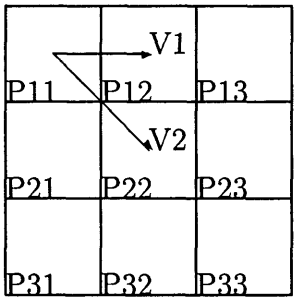

the higher order statistics may capture a feature of the data not readily apparent to the naked eye [8].

Normal Dispersion

Another method of estimating the roughness of the image is to find the average dispersion of the intensity surface normals across the image. The surface normal is defined as a line perpendicular to a surface at a particular point. For an intensity image, a surface can be fitted to a local group of pixels, and a normal to this intensity surface may be calculated. In order to find the average dispersion of surface normals, the surface normals at each pixel were calculated and compared to the surface normals at other pixels in the surrounding area. The area of the neighborhod was variable. For our images, we chose a 3×3 neighborhood of pixels. The image was separated into these 3 pixel by 3 pixel blocks with no overlap between the different blocks. Each 3×3 section was checked against the MAP image. If there were any pixels within the block that were shown to lie within a glare region, no calculation was done for that pixel block, since the whole region was assumed to be affected by glare.

For all the blocks not effected by glare, the following calculation was done for

each block. For each pixel in the block except those in the last row and column, we fit a plane to three points. The normal to the plane is the surface normal. For instance, the point in the top left corner of the above matrix is $P_{1,1}$. (see Figure 2.4) The normal vector was determined by the vectors $V1$ and $V2$. $P_{1,1}$ is located at $(1, 1, P11)$, $P_{1,2}$ is located at $(1, 2, P12)$, and $P_{2,2}$ is located at $(2, 2, P22)$ where the first number is the row position, the second is the column position, and the last is the pixel value at that point. Therefore, the vector $V1$ equals $(0, 1, P12 - P11)$ and $V2$ equals $(1, 1, P22 - P11)$. With two non-parallel lines, we can define a plane by taking the cross product of the two lines. Therefore, N equals $V1XV2$ where X indicates the cross product. We normalized the calculated normal vector in order to obtain a unit vector.

$$\hat{\mathrm{N}} = \frac{N}{\sqrt{N^T N}} \tag{2.31}$$

Once all the unit surface normals in a patch are calculated, the average direction for all surface normals in the patch could be obtained. Using the dot product, the angle between each surface normal and the average surface normal for a 3×3 patch can be calculated. Finally, the average average of these angles was calculated.

This process is repeated for each patch. The average angle calculated from all the patches may be used as a feature. It will be larger for rougher surfaces.

2.3.3 Color Features

Color is important in endoscopy because subtle alterations in color are often used to determine a site for biopsy [76]. Physicians have observed that adenomatous polyps are

"redder" than their surroundings, while hyperplastic polyps tend to be the same color as their surroundings. While researching polyps less than 5mm in size, Kronberg noted that hyperplastic polyps were light red with respect to the surrounding mucosa while adenomatous polyps were dark red with respect to the background [39]. This color variation was supported by Norfleet and later by Jaramillo [54, 32]. Iida made another interesting finding [29]. In Iida's study, researchers found that villous adenomas (the adenomas with the highest rates of carcinoma) were predominantly slightly reddish with white spots, which indicates that there may be a variation in the surface color among adenomatous polyps–particularly the ones with the highest chance of malignancy.

A researcher must be careful in quantifying color. Color perception is quite subjective. Perceived color depends not only on the color of the object being viewed but also on the color of the object's surroundings. This means, for example, that it becomes difficult to quantify the "redness" of an object. The question is raised: what does it mean for something to be "redder" than something else? An additional problem arises when the instruments used are not calibrated. In other words, something that looks red on one colonoscope may not appear to be the same red (or not red at all!) on another colonoscope. Of course, this means that some effort should be taken to avoid absolute color measures [75]. To solve this problem, different objects in the scene should be evaluated against one another. In the following set of features, we used the color of the mucosa surrounding the polyp as the object against which the polyp in the scene was evaluated. The features used in color differentiation are noted in Table 2.5. In the calculation of these features, if a pixel in the image was marked as glare in the MAP matrix, that pixel was excluded from the feature calculation.

Table 2.5: Color Features Considered in the Discrimination

FEATURE CLASS	FEATURE DESCRIPTION
Color	Chromaticity-Distance
Color	Chromaticity-Distance Ratio
Color	Retinex Coordinates-RG
Color	Retinex Coordinates-RB
Color	Variegated Color-mean
Color	Variegated Color-variance
Color	Variegated Color-mean ratio
Color	Variegated Color-variance ratio

Chromaticity Distance

Any pixel in an RGB color image may be mapped into a three-dimensional space. The three axes in that three-dimensional space correspond to the red, green, and blue values for the pixel. One way of looking at this arrangement is that the redder something becomes, the stronger will be its value along the red axis. In this section, we wished to test whether or not the color values on the polyp had larger average red values than the pixels in the background. To do this, we transformed the RGB coordinates into chromaticity coordinates which are defined as follows [73]:

$$r = \frac{R}{R+G+B} \tag{2.32}$$

$$g = \frac{G}{R+G+B} \tag{2.33}$$

$$b = \frac{B}{R+G+B} \tag{2.34}$$

This will normalize all the color values so that they lie between 0 and 1. This is important because, regardless of the brightness of the image, this will map the pixels onto the same triangle in color 3 space. A pure red color would correspond to a point lying on (1,0,0) (a maximum red value and zeros in green and blue). We define two rectangular subimages. One image, designated "foreground" lies on the polyp's surface. The second image, designated "background", lies on a section of the mucosa not containing the polyp. An example of a polyp image with the foreground (on the polyp) marked in black, and the background region marked in white is shown in Figure 2.5. For every pixel in the foreground

Figure 2.5: Polyp Image: Foreground and Background Marked

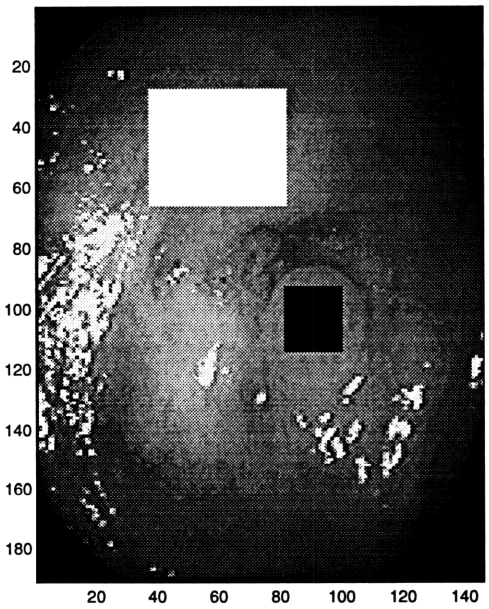

and background, we examined the distance between "pure" red point in chromaticity space and the pixel value using:

$$distance = \sqrt{(r-1)^2 + g^2 + b^2} \tag{2.35}$$

This calculation was carried out for every pixel in the polyp and the background except for those marked as glare. Once this was done, the average value for distance was found for on the polyp and in the background. The average value in the foreground was used as a feature. This value should be smaller for adenomas than for hyperplastic polyps. We also wanted to have a relative measure of color. Therefore, we took the ratio of the two values using the following equation:

$$RC_{metric} = \frac{averagedistance_{polyp}}{averagedistance_{background}} \tag{2.36}$$

This equation will take on values greater than 1 if the polyp is less red than the background, close to 1 if the polyp and background are the same color and less than 1 if the polyp is more red than the background.

Variegated Color

Another feature noted by observing the images was that the adenomatous polyps tended to be more uneven in color than the background. One reason for this to occur is that adenomatous polyps possess a visible surface texture while the hyperplastic polyps do not. We wanted to capture this color variegation in a feature. In order to capture this value, we took each color vector in RGB space and normalized it so that it corresponded to a direction in that space. For each pixel in the foreground and the background regions, the

following calculation was performed

$$\text{Color Vector} = \frac{1}{\sqrt{R_i^2 + G_i^2 + B_i^2}} \cdot \begin{bmatrix} R_i \\ G_i \\ B_i \end{bmatrix} \tag{2.37}$$

for $i = 1$ to the number of pixels in the area being considered (foreground or background). R_i, G_i, and B_i are the red, green, and blue values of a particular pixel. Then, a mean direction value was found for the foreground and the background using:

$$\widehat{RGB} = \begin{bmatrix} R_{avg} \\ G_{avg} \\ B_{avg} \end{bmatrix} = \frac{1}{P} \sum_{i=1}^{P} \begin{bmatrix} R_i \\ G_i \\ B_i \end{bmatrix} \tag{2.38}$$

for $i = 1$ to the number of pixels in the area being considered (foreground or background).

Once the average vector is calculated, the angle between every pixel in the area being considered and the average direction of all the vectors in that region can be found. The angle between each pixel direction can be calculated against the average pixel direction using

$$\theta_i = cos^{-1}([R_i G_i B_i] \cdot \begin{bmatrix} R_{avg} \\ G_{avg} \\ B_{avg} \end{bmatrix}) \tag{2.39}$$

for $i = 1$ to the number of pixels in the area being considered (foreground or background).

Once the angle has been calculated for each pixel in the region being inspected, Then, the mean and variance of the angle for all pixel values were calculated. These values were calculated for both the foreground and the background regions. The mean and variance of the angle of the foreground region were used as features. For relative feature, the ratio of the mean and variance of the foreground region to the background region (where the variation of the background region is the normalization factor) were used.

$$mean_{ratio} = \frac{mean_{polyp}}{mean_{background}} \tag{2.40}$$

$$variance_{ratio} = \frac{variance_{polyp}}{variance_{background}} \tag{2.41}$$

The mean and variance of the angle on the polyp will increase as the surface's color becomes more variegated. The values in the ratio will be greater than 1 when the polyp has more variegation than the background. Since the hyperplastic polyps resemble normal mucosa, their value should be nearly one (they should have the same level of variegation).

Retinex Theory

As noted previously, the color perception of a human observer is subjective. A quantitative description can be made using the color coordinates for which each coordinate value represents an intensity for the three primary colors (R,G,B). However, the perceived color of an observed region does not just depend on the measurement of light reflected from that region. It also depends on the effects of spectral intensities that emanate from all other areas of the scene. Research has found that higher-order mental processes in the brain

make use of this information to determine the perceived color of an area [41, 42, 43, 44]. One theory that has been used to investigate this effect is Retinex theory, introduced in equation form by Land [44]. This theory has three propositions: (1) Composition of light from an area in an image does not specify the perceived color of that area. (2) the perceived color of a unit area is determined by three numbers, each number is computed on a single waveband to give for that waveband the relationship between the unit area and the rest of the unit areas in the scene. (3) This trio of numbers, designated as $\hat{R}$, are computed by the retinex algorithm. $\hat{R}$ is the designator for the point in retinex three space, which specifies the perceived color of the unit area. This last assertion can be written in equation form in the following manner:

$$R(i,j) = \sum_{k} \delta \log\left(\frac{I_{k+1}}{I_k}\right) \tag{2.42}$$

where I_k is the intensity at position k in the image. R and I reference three vectors whose components are $R(1)$ which represents the long-wave components(red), $R(2)$ which represents the middle-wave components(green), and $R(3)$ which represents the short-wave components(blue). The quantity $\delta \log\left(\frac{I_{k+1}}{I_k}\right)$ is defined as

$$\delta \log\left(\frac{I_{k+1}}{I_k}\right) = \begin{cases} \log\left(\frac{I_{k+1}}{I_k}\right) & \left|\log\left(\frac{I_{k+1}}{I_k}\right)\right| > \epsilon \\ 0 & \left|\log\left(\frac{I_{k+1}}{I_k}\right)\right| < \epsilon \end{cases} \tag{2.43}$$

where ϵ is a small number ensuring changing spatial illuminations will not influence the results. This number was set to zero for this research.

In order to generate the coordinates in retinex three space, $R(i,j)$ was summed over N spatial paths starting from some background point and ending in the area in which

we want to find the color in retinex three space. This the following equation is used.

$$\overline{R}(i) = \frac{1}{N} \sum_{j=1}^{N} R(i,j) \tag{2.44}$$

Kienle investigated the simple question of why blood vessels appeared blue when viewed through the skin even though blood is known to be red [35]. In their experiments, they found that the retinex three space coordinates of the supposedly blue vessels actually lay in the red region in retinex three space. This corresponded to the long wave coordinate being "big" (>0) and the middle and short wave bands being small (<0). In standard retinex theory, one must look at the sum of spectral components in each band (long, medium, and short). Instead, Kienle made the approximation that one could examine single wavelengths (red, green, and blue) and found that good results were obtained using this approximation. This result is important in this thesis because the only data available was RGB endoscope images.

In this thesis, we wished to evaluate the "redness" of a polyp compared to the surrounding area. We decided that this meant that any point on the polyp should, in general, be perceived as "redder" than the background points. Therefore, we made the assumption that a number of lines could be drawn across the edges of the polyp. The lines of summation of a image are shown in black in Figure 2.6. By summing the results for these lines using the formulas described above, the interior of the polyp should be "redder" than the outside. Since the whole gastrointestinal tract is basically reddish in color, we need to evaluate a criteria for something to be "redder". We used the following: the greater the difference between the red band with the other two bands, the redder the area under

Figure 2.6: Polyp Image: Lines of Summation

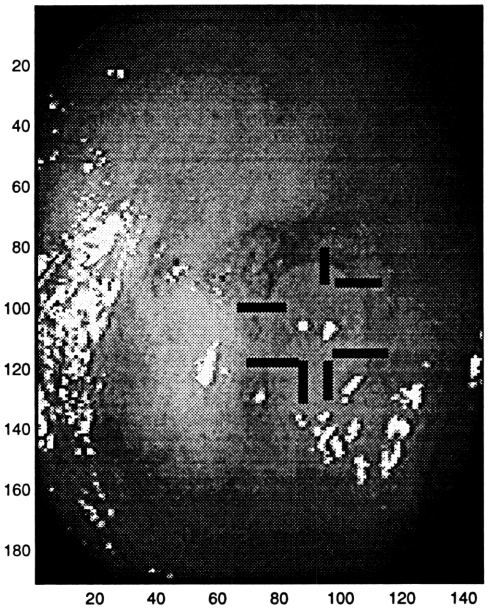

inspection. This required two metrics; one comparing the long and the medium band and the other comparing the long and the short band.

$$m_{RG} = \overline{R}(1) - \overline{R}(2) \tag{2.45}$$

and

$$m_{RB} = \overline{R}(1) - \overline{R}(3) \tag{2.46}$$

The more positive each of these metrics are, the more red should be the surface under observation compared to its surroundings.

2.3.4 Shape Features

Very little research has been done on investigating the shape of a polyp as viewed under the camera and its probability of being an adenomatous or hyperplastic polyp. This is understandable given the technical problems which arise when one attempts to do this. The first problem one confronts is segmenting the polyp from the image. For a side view of a pedunculated polyp (see Figure 2.7), it is not readily apparent where the stalk of the polyp ends and where the healthy mucosa begins. It is difficult to define where its

Figure 2.7: Polyp Image: Tubular Adenoma: Pose 1

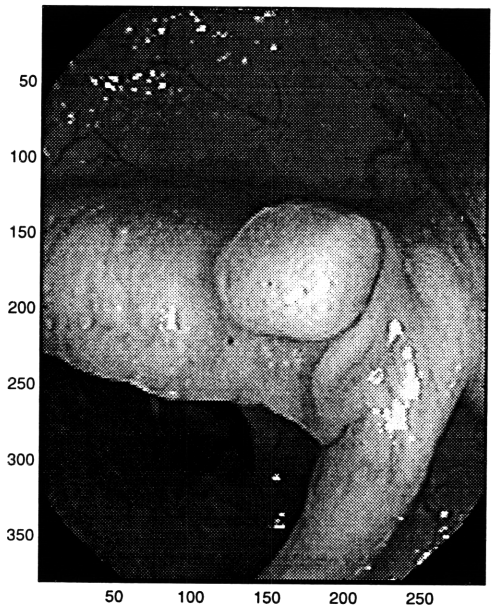

boundaries are. Any assumptions put into the shape finding algorithm (such as assuming smooth curves) will bias the results. Of course, even if this problem is solved, there is still the problem of pose. What angle will one use to view the polyp? A single polyp seen from different viewpoints can seem to have a very different shape. (see Figure 2.8) Assuming the

Figure 2.8: Polyp Image: Tubular Adenoma: Pose 2

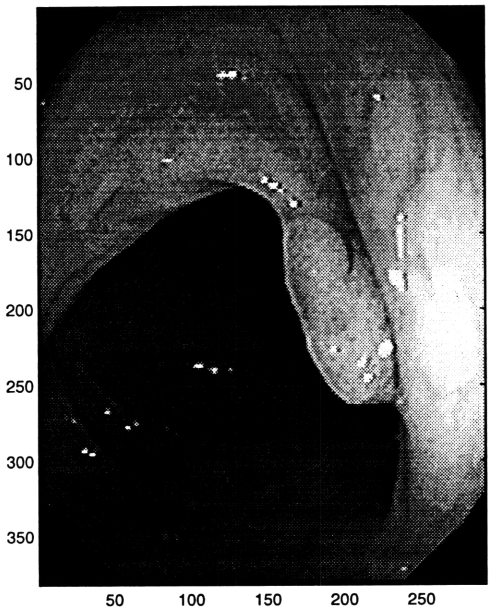

extraction problem and the pose problem are solved, there is still the problem introduced by the lens of the camera. Colonoscopes typically have very wide angle lens (usually around 120 degrees). This introduces a radial distortion into the image that alters the shape of objects being viewed. In order to correct for this, the camera must be calibrated to find the parameters to correct for this distortion. Once all these problems have been solved, an accurate estimate of shape can finally be made from the image.

Of course, if multiple images of a polyp are taken, another problem may arise. Polyps do not have a rigid shape, and they can be moved around by objects striking them. For example, during an examination, a physician might take one image of a polyp. Then, he might move the camera, brushing the polyp in the process, return the camera to the same position, and take another image of the polyp. The polyp may look quite different

between the two images.

For the reasons detailed above, a shape parameter was not evaluated as part of the discrimination in this thesis. However, it has yet to be determined if shape could be useful in differentiating among polyps.

Chapter 3

The Decision Algorithm

3.1 Overview of Algorithm

Statistical Analysis is defined as "a statistical technique for classifying individuals or objects into mutually exclusive and exhaustive groups on the basis of a set of independent variables." [16] Basic discriminant analysis can handle discrimination between two groups or among multiple groups. For this thesis, we only had to discriminate among two groups: adenomatous polyps and hyperplastic polyps. A linear discriminant can be used to generate a qualitative dependent variable from a set of independent variables. The independent variables are those features which we calculated in the last chapter. The following derivation for the linear discriminant used in this thesis was taken from Dillon and Goldstein and has been repeated here for clarity [16].

The purpose of discriminant analysis is to derive linear combinations of the independent variables that will be able to discriminate among the a priori defined groups in such a way that the misclassification error is minimized. This is accomplished by maximizing

the between-group variance relative to the within-group variance. Discriminant analysis can be thought of as a scoring system that assigns each group or object in a sample a score that is a weighted average of that group's or object's values on the set of independent variables (the features). Once the score is determined it may then be used to generate an a posteriori probability that determines the likelihood of that individual or object belonging to each of the groups.

The linear discriminant function will discriminate among the a priori defined groups in the "optimal" way. This "optimal" solution is defined as the result which will make the misclassification error rates obtained for a particular linear combination of variables smaller than the error obtained for any other linear combination. This optimality is dependent on two assumptions being met. These are (1) the p independent variables must have a multivariable normal distribution and (2) the $p \times p$ covariance matrix of the independent variables in each of the two groups must be the same [16]. Non-optimal results may be obtained if these assumptions are not met.

To summarize, the purpose of discriminant analysis is the assignment of objects into mutually exclusive and exhaustive groups.

3.2 Derivation of Decision Algorithm

Suppose a population, G, is made up of two groups G_1 and G_2. A measurement, X, consisting of p characteristics is observed from G. We wish to develop an assignment rule for X that will allocate this observation to G_1 or G_2. Of the n observations, the researcher knows that G_1 has n_1 observations and G_2 has n_2 observations.

A solution to this problem was provided by Fisher. Under the assumption of the true mean vector for G_i is $\mu_i, i = 1, 2$ and that the variance-covariance matrices $\sum_1$ and $\sum_2$ have a common value $\sum$, Fisher suggested that an optimal linear discriminant may be found by taking a linear combination of X such that the ratio of the differences in the means of the linear combinations in G_1 and G_2 to its variance is maximized. In other words, by denoting the linear combinations by $Y = b^T X$, we wish to find a vector of weights b so that we maximize the criterion

$$\Delta = \frac{b^T \mu_1 - b^T \mu_2}{b^T \sum b} \tag{3.1}$$

However, in most real problems, including the one discussed in this thesis, the parameters, μ and $\sum$ are not known. They must be estimated from the input data. Therefore, the n_i sample observations from each G_i are used to define a sample-based rule by replacing μ_i with $\overline{x}_i$ and $\sum$ with S. These estimates are given by:

$$\overline{x}_i^T = (\overline{x}_{i1}, \overline{x}_{i2}, ..., \overline{x}_{ip}) \tag{3.2}$$

where $i = 1, 2$ and

$$S = \frac{1}{n_1 + n_2 - 2}(x_1^T x_1 + x_2^T x_2) \tag{3.3}$$

where $\overline{x}_{ij} = \sum_{l=1}^{n_i} x_{jl}$, $i = 1, 2$ and $j = 1, 2, .., p$, and where x_1 is the $(p \times n_1)$ matrix of mean-normalized observations taken from G_1 and x_2 is the $(p \times n_2)$ matrix of observations in mean-normalized form taken from G_2. Replacing parameters with their sample-based estimates, setting the derivative of Δ equal to 0, and solving for b shows that

$$\hat{b} = S^{-1}(\overline{x}_1 - \overline{x}_2) \tag{3.4}$$

where S^{-1} is the inverse of the pooled sample variance-covariance matrix.

To summarize, we see that the discriminant function is a linear composite of the original measurements on which the sum of squared differences between the group means is maximal, relative to the within-groups variance. In the case of only two groups, a single function of the p measurements will account for all the differences.

With Fisher's linear discriminant function, the assignment rule that allocates individuals or objects to the two groups becomes the following: assign an individual or object with realized scores, x, on the p independent variables to G_1 if

$$|\hat{b}^T(x - \overline{x}_1)| \leq |\hat{b}^T(x - \overline{x}_2)| \tag{3.5}$$

or to G_2 if

$$|\hat{b}^T(x - \overline{x}_2)| < |\hat{b}^T(x - \overline{x}_1)| \tag{3.6}$$

3.3 Statistical Testing

One of the objectives of discriminant analysis is the determination of the extent to which the two a priori defined groups differ with respect to their average score profiles. One method for testing whether between-group differences are statistically significant is described below.

The mean value of the discriminant function is referred to as the group centroid. The group centroids, $\overline{Y}_i$, where i identifies the group being considered, are obtained by

applying the vector of discriminant coefficients to the mean score vector for each group, $\overline{Y}_i = \hat{b}^T \overline{x}_i$. The differences in group differences may be used to define Mahalanobis's generalized distance, D^2.

$$\overline{Y}_1 - \overline{Y}_2 = \hat{b}^T \overline{x}_1 - \hat{b}^T \overline{x}_2 \tag{3.7}$$

$$= (\overline{x}_1 - \overline{x}_2)^T S^{-1} \overline{x}_1 - (\overline{x}_1 - \overline{x}_2)^T S^{-1} \overline{x}_2 \tag{3.8}$$

$$D^2 = (\overline{x}_1 - \overline{x}_2)^T S^{-1} (\overline{x}_1 - \overline{x}_2) \tag{3.9}$$

D^2 can be used to determine if between group differences in mean score profiles are statistically significant. Large values of D^2 lead us to believe that the groups are sufficiently spread in terms of mean separation. A formal test can be constructed by forming

$$Z = \frac{n_1 n_2}{(n_1 + n_2)} \frac{(n_1 + n_2 - p - 1)}{(n_1 + n_2 - 2)p} D^2 \tag{3.10}$$

Under the hypothesis, H_0: $\mu_1 = \mu_2$ and common variance-covariance matrix the test statistic Z is distributed as an F-distribution with p and $n_1 + n_2 - p - 1$ degrees of freedom; that is

$$Z \sim F_{\alpha;(p,n_1+n_2-p-1)} \tag{3.11}$$

Using this relationship, we can define Hotelling's Two-Sample T^2-statistic to be

$$T^2 = \frac{n_1 n_2}{(n_1 + n_2)} D^2 \tag{3.12}$$

Using this relationship, H_0 is rejected at significance level α if

$$\frac{n_1 n_2}{(n_1 + n_2)} \frac{(n_1 + n_2 - p - 1)}{(n_1 + n_2 - 2)} (\overline{x}_1 - \overline{x}_2)^T S^{-1} (\overline{x}_1 - \overline{x}_2) > F_{\alpha;(p,n_1+n_2-p-1)} \tag{3.13}$$

where $F_{\alpha;(p,n_1+n_2-p-1)}$ denotes the upper α percentage points of the F-distribution with p and $n_1 + n_2 - p - 1$ degrees of freedom. The α statistic provides a useful metric to determine how well the two classes have been separated in the feature space.

Chapter 4

Real Data

4.1 Objective

Thus far, our investigation has focused on the techniques used to extract information from the endoscopic images. In chapter 3, we focused on the different features which may be of use in distinguishing different types of polyps and the clinical research which supported the use of those features. These features included the location of the polyp in the colon, the age of the patient, the size of the polyp as determined by histologic examination, texture features, and color features. We specified different image processing techniques which could prove useful in measuring these different qualities. In chapter 4, we described the decision algorithm which would be used to decide what type of polyp was being investigated. This algorithm, the linear discriminant algorithm, is first trained on a set of images for which the polyp's type is known. Based on this training set, it creates a discriminant to classify polyp images for which the type is not known. Of course, the true test of the work done in this thesis is to apply the approach described above to video endoscope data actually

taken from patients with adenomatous and hyperplastic polyps.

In this chapter, we test the techniques that we have developed in the previous chapters on actual polyp data. To do this, we put features from all classes in a single discriminant function in order to determine which class of features contributed the most to classification. We examined all possible combinations of features for sets of one feature, two features, three features, and four features. In order to pick the optimal reduced feature set for a particular number of features, the combination of features with the highest D^2 statistic was retained and all other combinations were discarded.

This chapter is organized as follows. First, we begin with a description of the real polyp data that is available to us. Then, we examine several algorithms that were used to preprocess the images. Finally, we evaluate sets of the input features using the linear discriminant in order to find some optimal set taken from all the classes of features.

4.2 Description of the Data

We are fortunate to have access to a set of polyp images taken during normal colonoscopy and the pathology reports that identify the type of polyp being examined for 62 polyps: 45 neoplastic polyps and 17 non-neoplastic polyps. These polyps are of varying types. The non-neoplastic polyps being considered are all hyperplastic polyps. The neoplastic polyps are of tubular adenomas, tubulo-villous adenomas, and villous adenomas. (see Figures 2.8, 4.9, and 2.2, respectively) The data set for each individual polyp consists of a series of endoscopic images of the polyp. The number of images for each polyp is variable. It could be as few as one, or it could consist of as many as 8 or 10 images. These images

are taken from a variety of viewing angles of the polyp, distances from the polyp, and lighting conditions. In the case wherein more than one polyp image was available to be processed, one of the images was chosen based on a qualitative assessment of the image's ability to convey the characteristics of the polyp. This assessment was based on minimum glare characteristics, good viewing distance, and a good viewing angle. The images were stored in TARGA format with 2 bytes allocated to each color pixel. This implies that there were 5 bits per color band. This translates to 32 different gray levels for the red, green, and blue bands. The images were of size 292 by 382 for high resolution images and half that in each dimension for the low resolution images. Images of both types were involved in the discriminant analysis. These images were taken with a number of different video endoscopes; no attempt was made to color calibrate the camera before the images of the polyps were acquired. Aside from the images, each polyp was also associated with a pathology report. This report contained the estimated location of the polyp in the patient's colon, the age of the patient, the dimensions of the polyp as estimated during biopsy, and the diagnosis of the polyp as determined during biopsy. As noted previously, histologic examination is the only clinically validated technique for diagnosing a colorectal polyp.

A semi-automated technique was used to determine what area of the polyp to examine for feature extraction. First, a rectangular area in the image was specified by the operator as lying entirely on the surface of the polyp. For relative color measures, a second rectangular area in the image was specified as just containing mucosa (not lying on the polyp or dark areas such as viewing deeper into the colon). Finally, a set of lines were chosen as crossing from the mucosa onto the surface of the polyp. These lines were used for the calculation in the retinex algorithm. The next preprocessing step was to process

the image in order to find areas corresponding to glare. These areas were identified so that they would not later be used during the feature extraction step. After specifying areas containing glare, three algorithms were applied to each input image. The first was an HSV enhancement technique. The second was a principal components transform to reduce the image from three color bands to one band containing a majority of the information from the original image. The last technique was unsharp masking. This was used to reduce the effect of variable lighting on the perceived texture on the surface of the polyp. After these three steps, the polyp image was ready for processing.

4.3 Accounting for Specular Reflection

There are many problems that arise when processing actual images and not just test data. Glare was one of these problems which arose when attempting to process the actual polyp images. The lighting element on the camera had the tendency of reflecting off the shiny sides of the intestinal wall. This created a problem because the sensor element (the CCD) of the camera would be saturated by the light reflecting from the surface under inspection (the polyp). In the regions of glare, the camera recorded only white. In these areas, there was no available information to be used for feature calculations. However, if these regions are ignored, they could create anomalies in the results. For instance, a texture calculation could read this area to be smooth when, in fact, it lay on the surface of a highly nodular adenomatous polyp. When possible, these features were distinguished from the rest of the image during feature calculation. This was not the case for radial frequency processing and for fractal dimension calculation. The glare effect was generally judged to be low frequency

and so was ignored for the radial frequency processing, since we were only concerned with the high frequency component of the signal. For fractal dimension calculation, we desired to have as large a region as possible to estimate the fractal dimension of the texture, and it was judged that if these regions were removed our area would become too small for effective estimation.

In order to delineate these areas in the image, a histogram was formed of all pixel values in the polyp image. The pixel locations containing the top 12% of all pixel values were declared to be in the glare region and marked. This threshold was found to work well experimentally. Since the regions of interest were dark spots (folds and grooves in the surface) or reddish spots, these areas could then be avoided when acquiring data.

In generating the algorithm to find the areas of glare in the image, two assumptions were made. The first was that, if glare affected a pixel, then that glare would be present in each band of the image. The second was that there would always be some glare in the image. The first assumption is validated by, if the CCD is saturated by intense white light in one band, then it will be saturated in all bands. The second assumption, though not guaranteed for all images (images do not need to have glare in them), was observed to be true for a large number of the images used in this thesis.

As detailed above, one may generate a distribution function for each color band. This distribution provides the percentage of the pixels that fall into each of the possible gray levels for the image. From this distribution, one may calculate a cumulative density function (CDF). This CDF tells us for any particular gray level in the image, what percentage of the pixels are at that gray level or less. If the probability of a particular gray level, g_i, is

equal to $p_u(g_i)$, then the CDF can be derived as follows:

$$P_u(u < g_i) = \sum_{i=0}^{g_i} p_u(g_i) \tag{4.1}$$

where $i = 0, 1, 2, ..., L-1$. L is the number of gray levels. Once the CDF is derived for the red, green, and blue bands, one may select an arbitrary threshold value of the image. The value 0.12 was observed to be a good threshold for the input images for this thesis. This meant that the top 12% of the pixel values were to marked as possible glare pixels in each band. The pixels that had been marked as glare in each band were indicated in a matrix, corresponding to that band which contained a 1 for a pixel that had been marked as glare and a 0 otherwise. These three matrixes were MAP_R, MAP_G, and MAP_B, corresponding to the red, green, and blue bands, respectively. By noting that glare would need to correspond to the pixel value being maxed out in each band, one can then write (where $\oplus$ indicates the logical and):

$$MAP = (MAP_R) \oplus (MAP_G) \oplus (MAP_G) \tag{4.2}$$

Therefore, if a pixel had been marked as glare in each band, then it corresponded to an area affected by glare. This MAP matrix was then used to determine what pixels in the image were processed for features.

An example of an image without glare marked is given in Figure 4.1. The same image with the glare marked is given in Figure 4.2.

Figure 4.1: Hyperplastic Polyp without glare marked

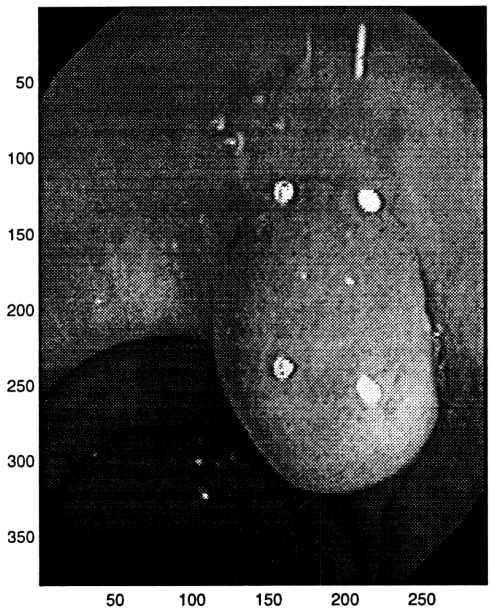

4.4 Principal Components Transform

There were three bands to be processed in the images that were examined, red, green, and blue. Even though having three bands was extremely useful for color image processing, it presented something of an ambiguity when considering what to process for the texture characteristics. As common sense tells us, the tissue of the human body reflects most strongly in the red band. This means that the red band will have the most reflected energy. However, there is so much reflected energy in the red band that most of the band is saturated or nearly so there is very little information to be used. (see Figure 4.3) This leaves the green band and the blue band. Another fact is that the sensitivity of the CCD in the camera is highest in the green band and lowest in the blue band. One can see the effect of the sensitivity of the camera in the following two pictures. The green band is observed

Figure 4.2: Hyperplastic Polyp with glare marked

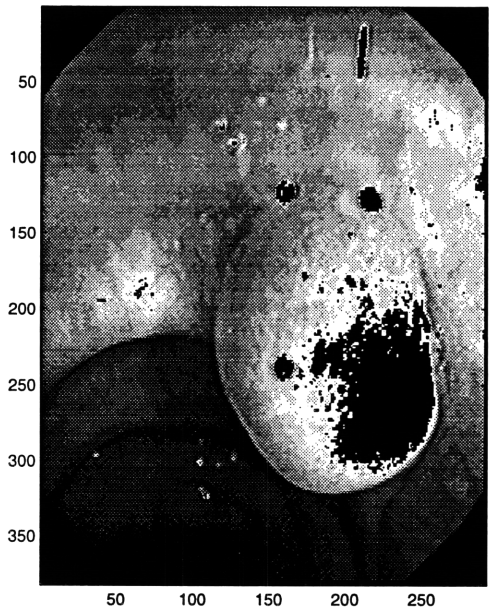

to have the highest amount of detail. (see Figures 4.4 and 4.5)

However, it did not make sense just to discard the red and blue bands. There was some information in them, just not the same amount as was in the green band. In order to take advantage of this information, we performed a principal components analysis of the entire image.

The Principal Components Transform (PCT) is based on the statistical properties of the image. In this thesis, the principal components transform is applied to the 3D color space. This method is described by Umbaugh [74]. The Principal Components Transform provides us with a data reduction technique that allows us to collapse the maximal information from the three color bands down into a single band.

In order to find the PCT for a particular image, the 3D color covariance must

Figure 4.3: Hyperplastic Polyp: Red Band

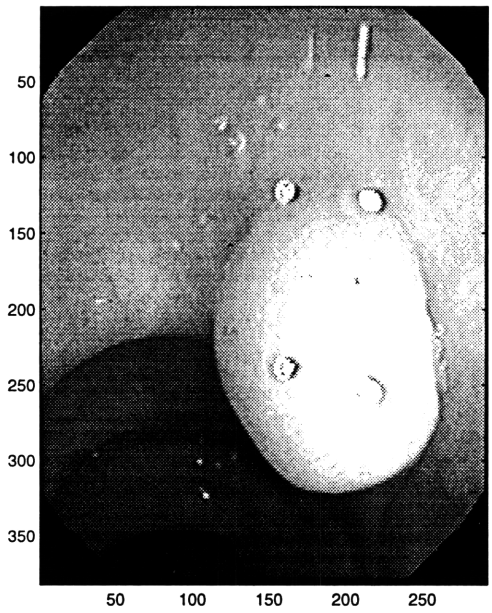

be found. This covariance matrix is defined as follows (where the R, G, and B labels apply to the Red, Green, and Blue images, respectively)

$$COV_{RGB} = \begin{bmatrix} C_{RR} & C_{GR} & C_{BR} \\ C_{RG} & C_{GG} & C_{BG} \\ C_{RB} & C_{GB} & C_{BB} \end{bmatrix} \tag{4.3}$$

where

$$C_{RR} = \frac{1}{P}\sum_{i=1}^{P}(R_i - m_R)^2 \tag{4.4}$$

Figure 4.4: Hyperplastic Polyp: Green Band

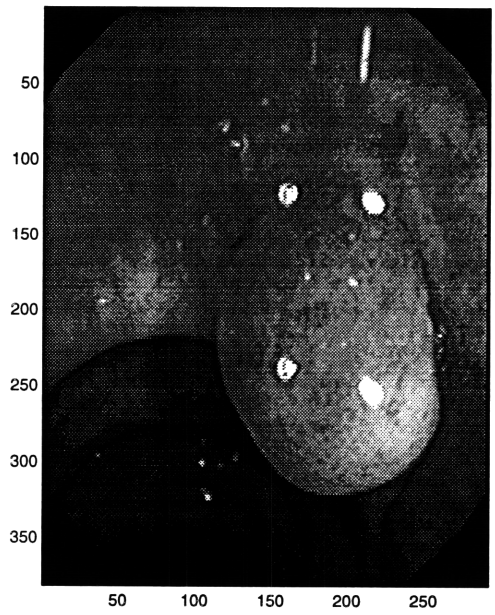

and P = number of pixels in the image and R_i = the red value for the ith pixel and

$$m_R = \frac{1}{P}\sum_{i=1}^{P} R_i \tag{4.5}$$

Similar equations are used for C_{GG} and C_{BB}. The cross-covariance terms, C_{GR}, C_{BR}, C_{RG}, C_{BG}, and C_{RB}, are defined as follows:

$$C_{XY} = \frac{1}{P}[\sum_{i=1}^{P} X_i Y_i] - m_X m_Y \tag{4.6}$$

with the means as defined above.

If the eigenvectors of the covariance matrix are used as a linear transform matrix on the original $[RGB]$ vectors, it can be shown that the resulting vectors have components

Figure 4.5: Hyperplastic Polyp: Blue Band

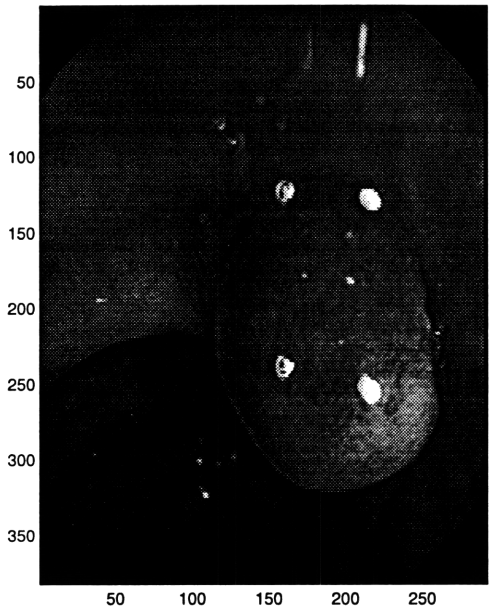

that are uncorrelated [16]. If the eigenvector corresponding to the largest eigenvalue is used for the transform then the variance in the data will be maximal. In other words, if $ev = [ev_R, ev_G, ev_B]$, the eigenvector corresponding to the largest eigenvalue can be used to linearly transform the entire color image to a single channel via

$$\begin{bmatrix} R_{2,i} \\ G_{2,i} \\ B_{2,i} \end{bmatrix} = \begin{bmatrix} ev_R & ev_G & ev_B \end{bmatrix} \begin{bmatrix} R_i \\ G_i \\ B_i \end{bmatrix} \tag{4.7}$$

where i is equal to one to the number of pixels in the image. If the output of this transform exceeded the maximum possible dynamic range of the original image, it was scaled down. The output of this algorithm for three images above is given in Figure 4.6.

Figure 4.6: Hyperplastic Polyp: Principal Components Transform

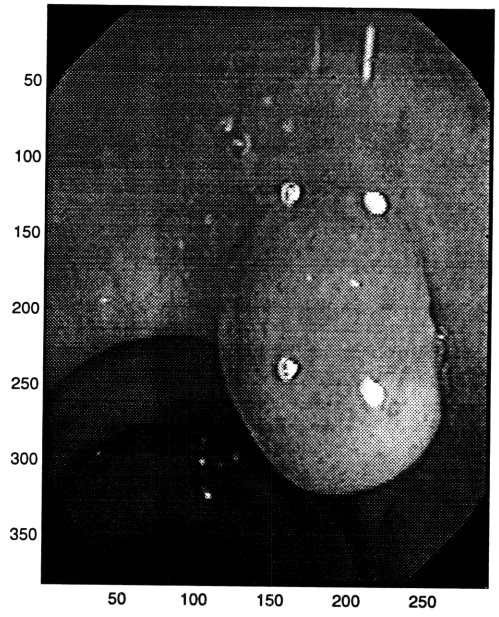

4.5 HSV Enhancement

HSV enhancement is a method of color image enhancement. With this method, first, an input RGB image is transformed into the HSV domain. Then, the S band is transformed by equalizing its histogram. With the RGB image, the three bands are red, green, and blue. In the HSV domain, the three bands are hue, saturation, and color value. The hue band refers to the color that the pixel most closely matches. The values of hue run from red to green to blue back to red. The saturation band controls the "purity" of the color. Low values of hue correspond to gray shades. Higher values of hue correspond to bright colors. Finally, color Value controls the overall brightness of the pixel. Low values of brightness correspond to dark (black) images [8].

The method of HSV image enhancement proceeds as follows. First, the input

image is transformed from the RGB to the HSV domain. In order to make the colors in the image more distinctive, we performed histogram equalization on the S band. To perform histogram equalization, the S band is histogrammed and a probability distribution, $p_u(x)$ is calculated. Once the probability distribution has been calculated, then a cumulative distribution can be derived from it. Then, the values in the cumulative histogram are spread apart so the values of S will cover the available space, accentuating differences between objects (and colors) in the image, where $P_u(x)$ is the cumulative distribution. An example of a histogram is given in Figure 4.7. An equalized version of the histogram is given in Figure 4.8. Notice how the values of the original space have been spread apart; making each one more distinctive. After this is done, the resulting HSV image is converted back to an RGB image for further processing. Figure 4.9 shows an image before HSV enhancement. Figure 4.10 shows the same image after processing.

Figure 4.7: Histogram: Unequalized

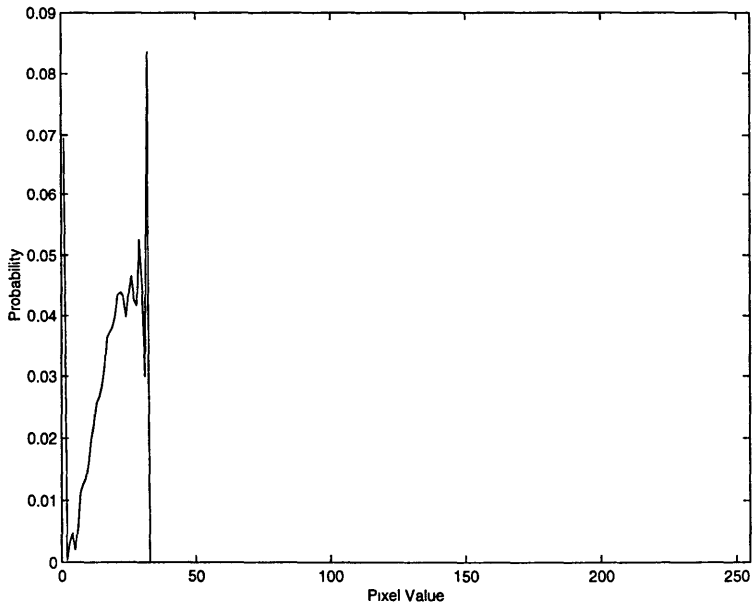

Figure 4.8: Histogram: Equalized

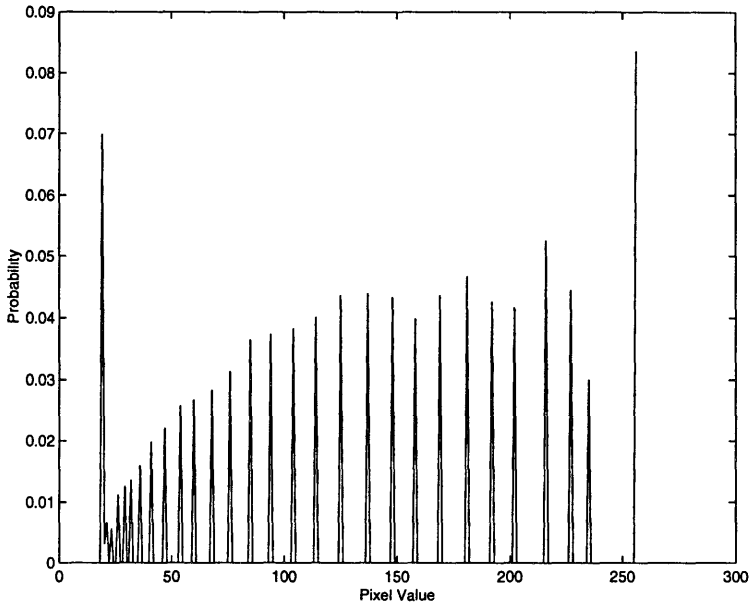

4.6 Unsharp Masking

The algorithm to perform unsharp masking is described below. There are three steps to the algorithm. First, the input image is low pass filtered. Next, this low-passed image is subtracted from the original image. This has the effect of removing the low frequency component of the image, while accentuating the high frequency details (such as edges). Then, the final output is shifted so that it lies within an acceptable range–such as within the range of the original image. The equations for the algorithm are detailed below:

An acceptable lowpass input mask, in this case, an averaging filter, is given

Figure 4.9: Tubulo-Villous Adenoma: Before HSV enhancement

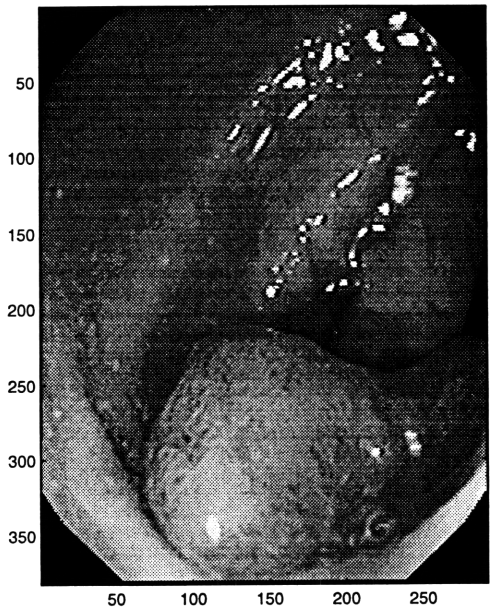

below. This format can be followed for masks with larger regions of support.

$$MASK = \frac{1}{9}\begin{bmatrix} 1 & 1 & 1 \\ 1 & 1 & 1 \\ 1 & 1 & 1 \end{bmatrix} \tag{4.8}$$

Then, the input signal is convolved with the MASK and the result is subtracted from the input.

$$OUTPUT = INPUT - MASK * INPUT \tag{4.9}$$

Finally, the output image is shifted so that its minimum pixel value is 0. If necessary, the dynamic range is then decreased so that the maximum pixel value is equal

Figure 4.10: Tubulo-Villous Adenoma: After HSV enhancement

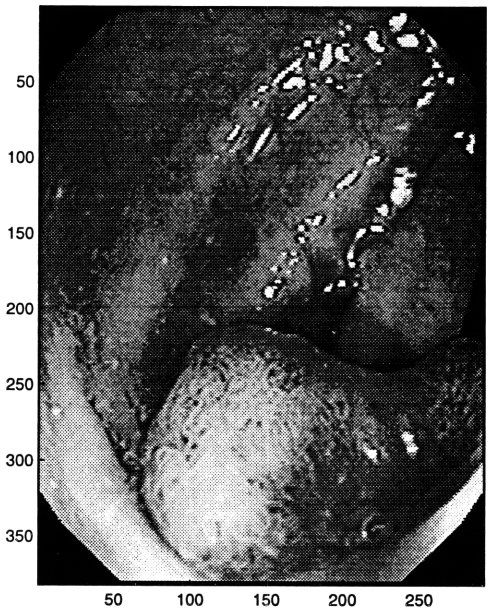

to 31.

4.7 Overall Performance

When a physician examines a polyp through a video endoscope, he does not take into account any one of the polyp's features when he attempts to classify the polyp. He is looking at the polyp's texture, color, and shape together. He is evaluating the size of the polyp to determine it is a threat to the patient by virtue of its size alone. He is also taking into account any one of a number of invisible factors which are difficult to quantify. Does this patient have a history of colorectal polyps? Does the patient's family? All of these factors are considered by the doctor before he makes a decision about the threat posed by a particular polyp. Research has shown that polyp's possess a number of characteristics

that may be used to classify them. There is no reason not to take into account all the available data when one is making a decision.

For this reason, we believe that a discriminant function should have access to as many factors as possible when it attempts to classify a polyp. In general, the more data that is available for an algorithm that better it will be able to perform. To this end, we decided to search the group of all features detailed in the previous sections for the combination of features that could most accurately classify a polyp as an adenoma or a hyperplastic polyp. A list of the features developed in previous chapters is given in Table 4.1.

The features obtained from the images were evaluated over a number of test runs. Each test run was split into two stages. During the first stage a number of training images were used to determine the optimal rule for the discriminant. Then, this optimal rule was applied to a set of test images in order to determine its performance for a set of data which it was not trained upon. A separate set of data was needed for the test set because a decision algorithm will become optimized to classify the data that it was trained upon. Testing an algorithm's performance with its training set will return optimistically biased results. We wished to simulate that the algorithm had been previously trained and was being used by a doctor in an examination. It is under these conditions that we are interested in the algorithm's performance. On every run, 30 of the 45 images of adenomatous polyps and 10 of the 17 images of hyperplastic polyps were used for the training stage of the algorithm. The remainder of the images was used for the test set. The images chosen for the training set and the test set were randomly determined at the beginning of each run in order to find the algorithm's performance for differing input. 5 runs were done to determine the

Table 4.1: Features Considered in the Discrimination

FEATURE NUMBER	FEATURE CLASS	FEATURE DESCRIPTION
1	Age	Patient's Age
2	Size	Volume of Polyp
3	Location	Location Found in the Colon
4	Color	Chromaticity-Distance
5	Color	Chromaticity-Distance Ratio
6	Color	Retinex Coordinates-RG
7	Color	Retinex Coordinates-RB
8	Color	Variegated Color-mean
9	Color	Variegated Color-variance
10	Color	Variegated Color-mean ratio
11	Color	Variegated Color-variance ratio
12	Texture	Fractal Dimension
15-19	Texture	Radial Frequency Bins
20	Texture	Normal Dispersion
21	Texture	Textural Edgeness-Sobel
22	Texture	Textural Edgeness-Laplacian
24	Texture	Histogram-Dispersion
25	Texture	Histogram-Variance
26	Texture	Histogram-Energy
27	Texture	Histogram-Skewness
28	Texture	Histogram-Kurtosis
29	Texture	Histogram-Entropy

variability of the results.

Each run was split into four parts. For a particular choice of training set, the algorithm was evaluated for all possible combinations of 1, 2, 3, and 4 features. For each number of features, the combination of features which provided the optimal discrimination power was chosen as the best combination of features for that number of features and training set. "Optimal" in this case was defined as the combination of features which returned the largest D^2 statistic. The D^2 statistic provides a sense of how separated the two different groups of data (adenomatous or hyperplastic) are in the feature space. In general, the higher the D^2 statistic the better will be the discrimination. Also, for the best combinations of features, an α statistic was calculated as described in Chapter 3.3. We want α to be small (<0.05) in order to show that between group differences are significant. Finally, the percentage of adenomatous and hyperplastic polyps classified correctly in both the training set and testing set were included. Results of the 5 test runs are given in Table 4.2. %AF denotes the percentage of adenomas classified correctly. %HF denotes the percentage of hyperplastic polyps identified correctly. %TF is the percentage of all polyps considered (hyperplastic and adenomatous polyps) identified correctly. The features chosen for each run are given in Table 4.3.

As Table 4.2 shows, as the number of features increased, the returned D^2 statistic increased as well. This was an expected result since we were optimizing our selection of features based off the D^2 statistic. However, for large values of D^2, where we would expect to receive perfect results on the discrimination, we found that we could still only find 80% of the polyps correctly. It also performed poorly when attempting to find the hyperplastic polyps in the testing set. As the number of features being considered increased,

Table 4.2: Algorithm Performance

Run 1	**Training Data**					**Test Data**		
Num Feats	%AF	%HF	%TF	D^2	α	%AF	%HF	%TF
1	63.3	70.0	65.0	0.64	0.0352	66.7	71.4	68.2
2	66.7	90.0	72.5	0.94	0.0431	66.7	57.1	63.6
3	70.0	70.0	70.0	1.21	0.0494	86.7	28.6	68.2
4	73.3	80.0	75.0	1.46	0.0579	73.3	28.6	59.1
Run 2	**Training Data**					**Test Data**		
Num Feats	%AF	%HF	%TF	D^2	α	%AF	%HF	%TF
1	66.7	1.00	75.0	1.38	0.0026	46.7	57.1	50.0
2	83.3	60.0	77.5	2.60	0.0005	53.3	42.9	50.0
3	83.3	70.0	80.0	2.79	0.0011	53.3	28.6	45.5
4	86.7	60.0	80.0	3.03	0.0021	66.7	42.9	59.1
Run 3	**Training Data**					**Test Data**		
Num Feats	%AF	%HF	%TF	D^2	α	%AF	%HF	%TF
1	70.0	60.0	67.5	0.75	0.0228	60.0	42.9	54.5
2	63.3	70.0	65.0	0.93	0.0444	53.3	42.9	50.0
3	63.3	90.0	70.0	1.33	0.0371	86.7	42.9	72.7
4	73.3	80.0	75.0	1.59	0.0437	73.3	42.9	63.6
Run 4	**Training Data**					**Test Data**		
Num Feats	%AF	%HF	%TF	D^2	α	%AF	%HF	%TF
1	63.3	70.0	65.0	0.61	0.0397	66.7	71.4	68.2
2	70.0	60.0	67.5	1.04	0.0312	80.0	57.1	72.7
3	80.0	70.0	77.5	1.24	0.0463	73.3	42.9	63.6
4	63.3	80.0	67.5	1.47	0.0575	80.0	28.6	63.6
Run 5	**Training Data**					**Test Data**		
Num Feats	%AF	%HF	%TF	D^2	α	%AF	%HF	%TF
1	70.0	80.0	72.5	1.04	0.0080	60.0	57.1	59.1
2	80.0	70.0	77.5	2.00	0.0021	60.0	28.6	50.0
3	76.7	80.0	77.5	2.39	0.0028	60.0	28.6	50.0
4	83.3	80.0	82.5	3.25	0.0013	66.7	14.3	50.0
Run Avg	**Training Data**					**Test Data**		
1	66.7	76.0	69.0	—-	——	60.0	60.0	60.0
2	72.7	70.0	72.0	—-	——	62.7	45.7	57.3
3	74.7	76.0	75.0	—-	——	72.0	34.3	60.0
4	76.0	76.0	76.0	—-	——	72.0	31.5	59.1

the performance of the training set (as measured by the total number of polyps diagnosed correctly) also tended to increase. Generally, the percentage of polyps found in the training set was between 65% and 82.5%. However, this behavior was not shared by the testing set. The performance of the algorithm on the testing set remained fairly constant throughout the run–regardless of the number of features being considered.

In this thesis, we explored metrics for three classes of features: pathology, color, and texture. As mentioned previously, the influence that the type of polyp had on this particular set of features was uncertain. Table 4.3 shows that the pathology features: patient's age, volume of the polyp, and location of the polyp in the colon, did not play a major role in the classification of the polyps for this experiment. This was somewhat surprising in the case of the volume of the polyp. It was expected that this would be able to discriminate among at least some of the sample polyps. This shows that, at best, polyp size should play a minor role in the discrimination, as we are interested in separating out those polyps of the same size that belong to different classes. Size may produce misleading results in this case.

Disappointingly, our results show that the color features explored in this thesis did not produce strong features. Color variegation, the retinex features, and the chromaticity "redness" features were chosen several times by the algorithm but not consistently. It is possible that the features chosen for this thesis did not capture the color feature that has been observed by doctors. A number of factors may have contributed to this occurring. Our attempts to normalize the color from image to image may have been unsuccessful. Ideally, the endoscopic camera should be calibrated to some known color standard before every examination. This would ensure the colors observed in one camera would be like

Table 4.3: Features Chosen for each Run

Run 1	
Num Feats	Feature(s) Chosen
1	29
2	16,29
3	15,17,29
4	5,15,17,29
Run 2	
Num Feats	Features Chosen
1	26
2	19,26
3	9,19,26
4	19,21,23,26
Run 3	
Num Feats	Features Chosen
1	12
2	12,26
3	12,27,28
4	3,12,27,28
Run 4	
Num Feats	Features Chosen
1	29
2	15,29
3	8,15,29
4	6,7,16,29
Run 5	
Num Feats	Features Chosen
1	29
2	24,29
3	6,24,29
4	6,7,24,29

those observed in another camera. In the case of the images used in this thesis, color calibration was not done on the camera's beforehand. In the absence of this calibration, another solution would be, before every examination, to image a color chart, where the colors on the chart are known. These images do exist, but they were not made available during the development stage of this algorithm so they were not used.

At each stage in the algorithm, texture was the class of feature chosen as having the greatest discrimination ability. Intuitively, this meets our expectations. As has been mentioned previously, the gold standard in polyp discrimination remains to be histology–an analysis of the microstructure of the polyp. Since this microstructure affects the macrostructure of the polyp, we expect texture to be important to our discriminant. Moreover, doctors using magnifying endoscopes and dye to more clearly visualize the macrostructure of polyps have reported good results. The strongest texture features were those associated with the fractal dimension of the polyp's surface, the radial frequency response and those that interpreted the distribution of the pixel values on the polyp, particularly those such as energy and entropy which measure how spread out the pixels are across all possible pixel values. This shows that a generic measure of roughness does capture the differences in texture between the two classes of polyps.

The results of this algorithm show that texture is important in discriminating between classes of polyps than are features related to color or pathology. It is unfortunate that we were not able to consider more features in the discriminant. In order to test the whole feature set, we would have needed 260 images in the training set just to evaluate the 26 features. More images would be needed for testing. Unfortunately, we had only 62 images available to us, and only 17 of the 62 images were of hyperplastic polyps. It is possible that

there were simply just not enough samples of hyperplastic polyps to properly characterize that group of polyp for the discriminant. This would explain why the algorithm could perform well on the training set and not be able to perform just as well on the testing set. A larger population of samples will be needed to fully evaluate the ability of this algorithm to classify polyps.

Chapter 5

Conclusions and Future Work

5.1 Conclusions

In this thesis, we have presented a method to apply pattern recognition and image processing techniques to the problem of estimating the potential malignancy of a colorectal polyp from an image and from data known a priori. This in vivo method provides an alternative to current ex vivo histological techniques. By estimating the potential malignancy of a polyp from colonoscope images, the process of polyp diagnosis becomes safer and more cost effective. In addition, our technique will give physicians information as to the most important features for diagnosis of a polyp.

In chapter 3, we explored the features which can be of use in distinguishing between types of polyps. These features took into account the limitations caused by the images: relatively low resolution and the possibility of glare effecting our results. The features we examined included age of the patient, size of the polyp, texture of the polyp's surface, and the color of the polyp compared with that of the surrounding mucosa. The

features were formulated in such a way that the results would be easily applicable to real data.

In chapter 4, we created a framework to make a diagnosis about the type of polyp under examination. This model, the linear discriminant, is a multivariate data reduction technique which is useful in collapsing a large number of measurements down into a single variable upon which to make a decision. The large number of measurements in this case were the features detailed in chapter 3. The D^2 statistic allows us to determine the effectiveness of the training set in separating the feature space.

In chapter 5, we applied the methods developed in the last two chapters to images of actual polyps. For each polyp image, a feature vector was calculated. Then, the image set was separated into two groups: a test image set and a training image set. The training image set was used to train the classifier, the test set was used to evaluate its performance. It was found that texture played the most important role in the discrimination. We were able to correctly classify 65% to 82.5% of the images viewed in the training set. Performance in the test set was more variable. On the average, we were able to classify about 60% of the test images correctly, which is only slightly better than guessing. We believe that a larger sample size will better characterize the two groups of polyps and lead to improved algorithm performance.

5.2 Future Work

During this research, it came to our attention that there were certain areas that could be explored in the future to enable our algorithm to return more robust results.

The data set available in this thesis was fairly small and did not contain a very large sampling of polyps. It would be beneficial for a larger data set to be available for follow up work. This would allow a larger number of features to be statistically significant during the training of the algorithm. Moreover, in these additional sample images, the optimal viewing distance should be maintained between the camera and the polyp and glare on the surface of the polyp should be minimized. It would be interesting to see how this algorithm faired with data provided by the newer magnifying colonoscopes.

Additional features could be incorporated into the discriminant in order to test their ability to distinguish between different types of polyps. These features could include new ways of measuring the texture and color. The techniques described in this thesis are just a small set of the possible measurements that could be made. Interesting research has been into evaluating the concentration of blood flow in an area through the use of endoscopic measurements. Thus far, the research has not attempted to evaluate the blood flow in polyps, but perhaps such a measurement would be useful [30, 63, 72]. Also, new categories of features could be examined. For instance, shape was not utilized in this thesis. Properly examined, shape may play a useful role in polyp diagnosis. In addition, different features could change their weights if some other feature is found. For instance, villous adenomas have higher cancer risks for smaller polyp sizes. If a polyp can be identified as a villous in structure, its size feature could increase in weight to reflect this.

The feature selection algorithm used in this thesis was computationally quite expensive. As the size of the subset of features being considered increases, the computations required to find the optimal reduced feature set rapidly become prohibitive. There are a number of stepwise selection procedures available which could be implemented to make the

search for a larger "optimal" set of features more feasible. This would allow a larger number of features to be considered in the discriminant and improve algorithm performance.

Since the features described in this thesis could be used to distinguish between a small set of objects found in the human body, it is our hope that they could be generalized to distinguish among a large set of objects in the human body (such as among several different types of polyps).

Finally, different algorithms could be explored in classifying the polyps. A linear discriminant was used in this thesis. However, there are a number of other methods available, such as neural networks, that may be able to provide more robust results for the available data set.

Bibliography

[1] K. Araki, M. Kobayashi, T. Ogata, "A Scanning Electron Microscopic Study of the Three-Dimensional Configuration of Isolated Crypts from Human Colon Adenomas," *Med. Electron Microsc*, 27(1):55-60, 1994.

[2] K. Araki, T. Ogata, M. Kobayashi, R. Yatani, "A Morphological Study of the Histogenesis of Human Colorectal Hyperplastic Polyps," *Gastroenterology*, 109:1468-74, 1995.

[3] A. Axelrad, D. Fleischer, A. Geller, C. Nguyen, J. Lewis, F. Al-Kawas, M. Avigan, A. Montogomery, S. Benjamin, "High-Resolution Chromoendoscopy for the Diagnosis of Diminutive Colon Polyps: Implications for Colon Cancer Screening," *Gastroenterology*, 100:1253-8, 1996.

[4] D. Ballard, C. Brown, *Machine Vision*, Prentice-Hall, Inc., 1982.

[5] J. Beard, "Improved Image for Endoscopy," *New Scientist*, Vol 111:22, Aug 1986.

[6] P. Bond, ed., "Focus on Endoscopy," *Health Devices*, 23(5), 1994.

[7] G. Bottiroli, A. Croce, D. Locatelli, R. Marchesini, E. Pignoli, et al., "Natural Flourescence of Normal and Neoplastic Human Colon," *Lasers in Surgery and Medicine*, 16:48-60, 1995.

[8] K. Castleman, *Digital Image Processing*, Prentice Hall, 1996.

[9] Y. Carts-Powell, "Endoscopic Imaging Allows Optical Biopsy," *Laser Focus World*, 33, Sept 97.

[10] M. Catalano, M. Sivak Jr., R. Van Stolk, G. Zuccaro Jr., T. Rice, "Initial Evaluation of a New- Generation Endoscopic Ultrasound System," *Gastrointest. Endosc.*, 40(3):356-9, 1994.

[11] A. Chak, M. Sivak, "Electronic Endoscopy, Blood Flow Measurement, and Autofluourescence Tissue Spectroscopy," *Endoscopy*, 26(1):169-74, 1994.

[12] C. Chen, J. Daponte, M. Fox, "Fractal Feature Analysis and Classification in Medical Imaging," *IEEE Trans on Medical Imaging*, 8(2):133-42, 1989.

[13] R. Cothren, R. Richards-Kortum, M. Sivak, et al., "Gastrointestinal Tissue Diagnosis by Laser-Induced Flourescence Spectroscopy at Endoscopy," *Gastrointestinal Endoscopy*, 36(2):105-11, 1990.

[14] J. Cronstedt, L. Carling, R. Willen, J. Ericsson, L. Svedberg, "Geographic Differences in the Prevalence and Distribution of Large-Bowel Polyps – Colonoscopic Findings," *Endoscopy*, 19:110-3, 1987.

[15] S. Cross, J. Bury, P. Silcocks, T. Stephenson, and D. Cotton, "Fractal Geometric Analysis of Colorectal Polyps," *Journal of Pathology*, Vol. 172:317-23,1994.

[16] W. Dillon, M. Goldstein, *Multivariate Analysis: Methods and Applications*, John Wiley and Sons, Inc., 1984.

[17] B. Dubuc, S. Zucker, C. Tricot, J. Quiniou, D. Wehbi. "Evaluating the Fractal Dimension of Surfaces," *Proc of the Royal Society of London, Series A*, 425:113-27, 1989.

[18] C. Fortin, R. Kumaresen, W. Ohley, S. Hoefer, "Fractal Dimension in the Analysis of Medical Images," *IEEE Eng. in Med. and Biol.*, 11(2):65-71, 1992.

[19] C. Frank, R. McCreery, D. Redd, "Raman Spectroscopy of Normal and Diseased Human Breast Tissues," *Anal. Chem.* 67:777-83, 1995.

[20] M. Fujino, T. Kawai, A. Morozumi, Y. Yamamoto, M. Ikeda, H. Suzuki, "Endoscopic Image Manipulation: State of the Art," *Endoscopy*, 24(2):516-21, 1992.

[21] M. Fujino, A. Morozumi, T. Nakamura, Y. Kojima, T. Kawai, T. Sato, K. Kubo, et al., "Electronic Endoscopy in Perspective," *J. Gastroenterol*, 29(7):85-90, 1994.

[22] J. Gagnepain, C. Roques-Carmes, "Fractal Approach to Two-Dimensional and Three-Dimensional Surface Roughness," *Wear*, 109:119-26, 1986.

[23] D. Gorsich, C. Tolle, "Wavelet and Fractal Analysis of Ground Vehicle Images," *SPIE*, 2825:109-119, 1996.

[24] R. Haralick, L. Shapiro, *Computer and Robot Vision, Vol. 1*, Addison-Wesley, 1992.

[25] B. Hofstad, M. Vatn, S. Larsen, H. Huitfeldt, M. Osnes, "In situ Measurement of Colorectal Polyps to Compare Video and Fiberoptic Endoscopes," *Endoscopy*, 26(5):461-5, 1994.

[26] J. Huang, D. Turcotte, "Fractal Image Analysis: Application to the Topography of Oregon and Synthetic Images," *J. Opt. Soc. Am. A.*, 7(6):1124-30, 1990.

[27] Q. Huang, J. Lorch, R. Dubes, "Can the Fractal Dimension of Images be Measured?" *Pattern Recognition*, 27(3):339-48, 1994.

[28] M. Iida, A. Iwashita, T. Yeo, et al., "Villous Tumors of the Colon:Correlation of Histologic, Macroscopic, and Radiographic Features," *Radiology*, 167:673-7:1988.

[29] M. Iida, A. Iwashita, T. Yao, S. Kitagana, K. Sakatomo, M. Fujishima, "Endoscopic Features of Villous Tumors of the Colon: Correlation with Histological Findings," *Hepato-Gastroenterol*, 37:342-4, 1990.

[30] R. Jacoby, F. Zwiebel, R. Herpers, K. Englmeier, "Estimation of Blood Flow in the Upper Gastrointestinal Tract by Analysis of Endoscopic True Color Images," *MEDINFO Proc.*, 714-7, 1995.

[31] A. Jain, *Fundamentals of Digital Image Processing*, Prentice Hall, 1989.

[32] E. Jaramillo, M. Watanabe, P. Slezak, C. Rubio, "Flat Neoplastic Lesions of the Colon and Rectum Detected by High-Resolution Video Endoscopy and Chromoscopy," *Gastrointest Endosc*, 42(2):114-22, 1995.

[33] C. Kapadia, F. Cutruzolla, K. O'Brien, M. Stetz, R. Enriquez, L. Deckelbaum, "Laser-Induced Flourescence Spectroscopy of Human Colonic Mucosa," *Gastroenterology*, 99:150-7, 1990.

[34] K. Kincaid, "Optical Diagnostics Image Tissues and Tumors," *Laser Focus World*, 71-81:Feb 1996.

[35] A. Kienle, L. Lilge, I. Vitkin, M. Patterson, B. Wilson, R. Hibst, R. Steiner, "Why do Veins Appear Blue? A New Look at an Old Question," *Applied Optics*, 35(7):1151-60, 1996.

[36] K. Knyrim, H. Siedlitz, N. Vakil, F. Hagenmuller, M. Classen, "Optical Performance of Electronic Imaging Systems for the Colon," *Gastroenterology*, 96(3):776-82, 1989.

[37] K. Knyrim, H. Siedlitz, N. Vakil, "Current Developments in Electronic Endoscopy," *Endoscopy*, 24(suppl 2):502-5, 1992.

[38] K. Kousen, H. Takahashi, M. Seki, R. Fujita, F. Sugata, K. Namatame, "Computer Analysis of Fine-Network Pattern of the Gastric Mucosa via Electronic Endoscope," *Progress of Digestive Endoscopy*, 32:100-3, 1988.

[39] O. Kronberg, E. Hage, "Hyperplasia or Neoplasia: Macroscopic Vs. Microscopic Appearance of Colorectal Polyps," *Scand J. Gastroenterol*, 20:512-5, 1985.

[40] S. Kudo, S. Tamura, T. Nakajima, H. Yamano, H. Kusaka, H. Watanabe, "Diagnosis of Colorectal Tumorous Lesions by Magnifying Endoscopy," *Gastrointestinal Endoscopy*, 44(1):8-14, 1996.

[41] E. Land, J. McCann, "Lightness and Retinex Theory," *J. Opt. Soc. Am.*, 61:1-11, 1971.

[42] E. Land, "The Retinex Theory of Color Vision," *Sci. Am.*, 237:108-28, 1977.

[43] E. Land, "An Alternative Technique for the Computation of the Designator in the Retinex Theory of Color Vision," *Proc. Natl. Acad. Sci.* 83:3078-80, 1986.

[44] E. Land, "Recent Advances in Retinex Theory," *Vision Res.* 26:7-21, 1986.

[45] B. Levin, G. Murphy, "Revision in the American Cancer Society: Recommendations for the Early Detection of Colorectal Cancer," *Cancer*, 42:296-9, 1992.

[46] C. Macaulay, P. Palcic, "Fractal Texture Features Based on Optical Density Surface Area," *Analytical and Quantitative Cytology and Histology*, 12(6),394-8, 1990.

[47] R. Marchesini, M. Brambilla, E. Pignoli, G. Bottiroli, et al., "Light-Induced Flourescence Spectroscopy of Adenomas, Adenocarcinomas, and Non-Neoplastic Mucosa in Human Colon," *J. Photochem. Photobiol. B: Biol.*, 14:219-30, 1992.

[48] R. Marchesini, E. Pignoli, S. Tomatis, S. Fumagalli, A. Sichirolli, et al., "Ex Vivo Optical Properties of Human Colon Tissue," *Lasers in Surgery and Medicine*, 15:351-7, 1994.

[49] C. Margulies, B. Krevsky, M. Catalano, "How Accurate are Endoscopic Measurements of Size?" *Gastrointest Endoscop*, 40(2 pt 1):174-7, 1994.

[50] K. Miyokawa, R. Owoc., "Electronic Imaging Technology Revolutionizes Surgical Procedures," *Laser Focus*, Vol 23:116-7, Aug 1987.

[51] S. Mughal, M. Filipe, J. Jass, "A Comparative Ultrastructural Study of Hyperplastic and Adenomatous Polyps, Incidental and in Association with Colorectal Cancer," *Cancer*, 48:2746-55, 1981.

[52] P. Newcomb, R. Norfleet, B. Storer, T. Surawicz, P. Marcus, "Screening Sigmoidoscopy and Colorectal Cancer Mortality," *J Natl Cancer Inst*, 84:1572-1575, 1992.

[53] K. Nishimura, Y. Niwa, H. Goto, S. Hase, T. Arisawa, T. Hayawaka, "Three-Dimensional Ultrasonagraphy of Gastroinestinal Lesions using an Ultrasound Probe," *Scand J. Gastroenterol.*, 32(9):862-8, 1997.

[54] R. Norfleet, M. Ryan, J. Wyman, "Adenomatous and Hyperplastic Polyps Cannot be Reliably Distinguished by their Appearance through the Fiberoptic Sigmoidoscope," *Dig Dis Sci*, 33(9):1175-7, 1988.

[55] N. Ohyama, T. Suzuki, T. Honda, J. Tsujiuchi, "Digital Processing of Endoscopic Color Images," *Optics Communications*, 55:242-7, 1985.

[56] S. Peleg, J. Naor, R. Hartley, D. Avnir, "Multiple Resolution Texture Analysis and Classification," *IEEE Trans on Pattern Analysis and Machine Intelligence*, 6(4):518-23, 1984.

[57] T. Peli "Multiscale Fractal Theory and Object Characterization," *J. Opt. Soc. Am. A.*, 7(6):1101-12, 1990.

[58] A. Pentland, "Fractal-Based Description of Natural Scenes," *IEEE Trans on Pattern Analysis and Machine Intelligence*, 6(6):661-74, 1984.

[59] L. Picciano, J. Taylor, "Color Technology in Video Endoscopy," *Journal of Clinical Engineering.* 19(6):490-6, Nov/Dec 1994.

[60] D. Ransahoff, C. Lang, "Sigmoidoscopic Screening in the 1990's," *JAMA*, 269:1278-81, 1993.

[61] A. Rao, *A Taxonomy for Texture Description and Identification*, Springer-Verlag New York, Inc, 1990.

[62] J. Rey, M. Albuisson, M. Greff, J. Bidart, J. Monget, "Electronic Video Endoscopy: Preliminary Results of Imaging Modification," *Endoscopy* 20(1):8-10, 1988.

[63] N. Sato, S. Tsuji, S. Kawano, N. Hayashi, M. Tsujii, Y. Ishigami, T. Ohihara, K. Nagano, T. Kamada, "Computer-Assisted Two-Dimensional Analysis of Gastric Mucosal Hemoglobin Distribution using Electronic Endoscopy," *Endoscopy*, 24(suppl 2):522-6, 1992.

[64] H. Schepers, J. van Beek, J. Bassingthwaighte, "Four Methods to Estimate the Fractal Dimension from Self-Affine Signals," *IEEE Eng in Med and Bio*, 11(2):57-65, 1992.

[65] J. Selby, G. Friedman, C. Quesenberry, N. Weiss. "A Case-Control Study of Screening Sigmoidoscopy and Mortality from Colorectal Cancer," *N Engl J Med*, 326:653-7: 1992.

[66] H. Siedlitz, M. Classen, "Optical Resolution and Color Performance of Electronic Endoscopes," *Endoscopy*, 24(3):225-8, 1992.

[67] A. Chak, M. Sivak, "Electronic Endoscopy, Blood Flow Measurement, and Autoflourescence Tissue Spectroscopy," *Spectroscopy*, 26(1):169-74, 1994.

[68] M. Sleisinger, J. Fordtran, ed, *Gastroinstestinal Disease, 4th ed.*, W.B. Saunders Company, 1989.

[69] W. Swobodnik, "Mechanics of Image Manipulation," *Gastroenterologist*, Dec 3(4),266-7, 1995.

[70] G. Tearney, M. Brezinski, B. Bouma, S. Boppart, C. Pitris, J. Southern, J. Fujimoto, "In Vivo Endoscopic Optical Biopsy with Optical Coherence Tomography," *SCIENCE*, 276:2037-9, 1997.

[71] J. Theiler, "Estimating Fractal Dimension," *J. Opt. Soc. Am. A*, 7(6):1055-73, 1990.

[72] S. Tsuji, S. Kawano, H. Hayashi, M. Tsuji, T. Ogihara, T. Kamada, N. Sato, "Analysis of Mucosal Blood Hemoglobin Distribution in Gastric Ulcers by Computerized Color Display on Electronic Endoscopy," *Endoscopy*, 23:321-4, 1991.

[73] S. Umbaugh, R. Moss, W. Stoecker, "Automatic Color Segmentation of Image with Application to Detection of Variegated Coloring in Skin Tumors," *IEEE Eng. in Med. and Biol. Mag.*, 89:43-52, 1989.

[74] S. Umbaugh, R. Moss, W. Stoecker, "An Automatic Color Segmentation Algorithm with Application to Identification of Skin Tumor Borders," *Comp. Med. Imaging and Graphics*, 16(3):227-35, 1992.

[75] S. Umbaugh, *Computer Vision and Image Processing: A Practical Approach Using CVIP Tools*, Prentice- Hall, 1998.

[76] N. Vakil, K. Knyrim, E. Everback, "The Appreciation of Colour in Endoscopy," *Bailliere's Clinical Gastroenterology*, 5(1):183-94, 1991.

[77] N. Vakil, K. Knyrim, "Electronic Imaging Technology," *Gastrointestinal Endoscopy Clinics of North America*, 4(3):463-73, 1994.

[78] N. Vakil, K. Bourgeois, "A Prospective, Controlled Trial of Eight-Bit, 16-Bit, and 24-Bit Digital Color Images in Electronic Endoscopy," *Endoscopy*, 27:589-92, 1995.

[79] N. Vakil, W. Smith, K. Bourgeouis, et al., "Endoscopic Measurement of Lesion Size: Improved Accuracy with Image Processing," *Gastrointest Endosc*, 40:178-83, 1994.

[80] A Verhest, R Kiss, D d' Olne, I Salmon, Y de Launit, C Fourneau, J Pasteels, and J Pector, "Characterization of Human Colorectal Mucosa, Polyps, and Cancers by Means of Computerized Morphonuclear Analysis," *Cancer*, 65(9),2047-54, 1990.

[81] T. Yamada, ed., *Textbook of Gastroenterology, Vol I,II*, J.B. Lippincott Company, 1991.

[82] Y. Yang, G. Tang, M. Bessler, R. Alfano, "Flourescence Spectroscopy as a Photonic Pathology Method for Detecting Colon Cancer," *Lasers in Life Sciences*, 6(4):259-76, 1995.